

Spectroscopic observations of comet C/1999 H1 (Lee) with the SEST, JCMT, CSO, IRAM and Nançay radio telescopes

26 May 2000

N. Biver ¹, D. Bockelée-Morvan ², J. Crovisier ², F. Henry ², J.K. Davies ³, H.E. Matthews ³, P. Colom ², E. Gérard ², D.C. Lis ⁴, T.G. Phillips ⁴, F. Rantakyö ⁵, L. Haikala ⁵, and H.A. Weaver ⁶

ABSTRACT

Coordinated spectroscopic radio observations of comet C/1999 H1 (Lee) were undertaken between May 4 and October 26, 1999, using the Swedish-ESO Submillimetre Telescope, the James Clerk Maxwell Telescope, the Caltech Submillimeter Observatory, the 30-m telescope of the Institut de Radio Astronomie Millimétrique, and the Nançay radio telescope.

We report on observations of OH, HCN, CH₃OH, H₂CO, CS and on the evolution of their production rates with heliocentric distance, between 0.8 and 1.7 AU, where the total outgassing rate ranged between 0.2 and 1.6×10^{29} molecules s⁻¹. HNC was detected unexpectedly in this medium activity comet with a relatively large HNC/HCN mixing ratio of 12%, close to that measured in comet C/1995 O1 (Hale-Bopp), which cannot be explained by current chemical models of the coma. CO was tentatively detected with a low abundance around 4% relative to water and is clearly underabundant in comparison to comets Hyakutake and Hale-Bopp. An upper limit of D/H < 300×10^{-5} in water was found from a brief search for HDO.

Molecular abundances relative to water of the other species around 1 AU are similar to those observed in other comets, although CH₃OH (4%) and H₂CO (1%) exhibit some of the largest abundances compared to previous comets.

Subject headings: comets: general — comets: individual (C/1999 H1 (Lee)) — radio emission lines

1. Introduction

Comets are the repository of important information on the origin of our Solar System. Cometary nuclei have been stored at cold temperatures for most of the past 4.6 billion years and progressively release volatile species as they enter the inner Solar System. Radio observations enable the investigation of many of these molecules and, in particular, allow the determination of relative abundances that can yield information on the formation of cometary nuclei. C/1999 H1 (Lee), which has a highly inclined orbit (149°) and an orbital period longer than 80 000 years, belongs to the long-period comets, which are thought to have formed in the vicinity of the giant planets before being expelled to the Oort cloud in the outer Solar System. Discovered by Steven Lee (Lee & Garradd 1999) on April 16, 1999, comet C/1999 H1 offered a good opportunity to study an intrinsically active comet, which total outgassing

¹Institute for Astronomy, University of Hawaii, 2680 Woodlawn Drive, Honolulu, HI 96822, USA

²Observatoire de Paris-Meudon, 5, place J. Janssen, F-92195 Meudon, France

³Joint Astronomy Centre, 660 N. A'ohoku Place, Hilo, HI 96720, USA

⁴California Institute of Technology, MS 320-47, Pasadena, CA 91125, USA

⁵Swedish-ESO Submillimetre Telescope, ESO, Alonso de Cordova 3107, Vitacura, Santiago, Chile

⁶Johns Hopkins University, 3400 North Charles Street, Baltimore, MD 21218-2686, USA

rate exceeded 10^{29} molecules s^{-1} at perihelion, on July 11 at 0.71 AU from the Sun. The first perigee took place on May 5 at 0.72 AU from the Earth, and the second one on September 30 at 0.83 AU. Its visual magnitude peaked at ~ 6.5 in June 1999 and it remained brighter than 8th magnitude during the five month period (May–September) when we studied it at radio wavelengths. Since the extensive study of comets C/1996 B2 (Hyakutake) and C/1995 O1 (Hale-Bopp), the apparition of C/1999 H1 (Lee) represented the next available opportunity to undertake a comprehensive study of a comet, searching for species like CO, CS and HNC that were poorly studied before. In contrast to the situation for comets Hyakutake and Hale-Bopp, C/1999 H1 (Lee) immediately revealed from its first observations at the Swedish-ESO Submillimetre Telescope (SEST) on May 5, that it was rich in methanol, making it an especially interesting target. In addition, the H_2O production rate has been measured directly by the Submillimeter Wave Astronomical Satellite (SWAS) at 557 GHz (Neufeld et al. 2000), while S_2 has been detected with the Hubble Space Telescope (Feldman et al. 1999). Infrared observations from Mauna Kea yielded a secure detection of CO, as well as the detection of several molecules lacking dipole moments (C_2H_6 , CH_4 , C_2H_2) that cannot be studied at radio wavelengths (Mumma et al. 1999, Weaver et al. 1999).

We present here the result of a 5-month monitoring of comet Lee at submillimeter to centimeter wavelengths. The observations, presented in § 2, also provide information on the gas kinetic temperature and the evolution of the expansion velocity between 0.9 and 1.7 AU from the Sun (§ 3). Production rates and their evolution with heliocentric distance (r_h) are presented in § 4–5 and molecular abundances and their implications are discussed in § 6–8.

2. Observations

Comet Lee was first detected at radio wavelengths on May 4, 1999 with the SEST, and this was followed by the detection of OH with the Nançay radio telescope (NRT) on May 8. Subsequent observations at the James Clerk Maxwell Telescope (JCMT), Caltech Submillimeter Observatory (CSO) and Institut de Radio Astronomie Millimétrique (IRAM) 30-m telescope were scheduled on short notice as target-of-opportunity programs. The 18-cm OH lines in the comet were detected on a daily basis at the NRT between May 8 and June 20, but could not be detected later and post-perihelion (July 01–Aug.15) (Section 6, Table 7).

The comet was observed in 3 sessions at the SEST in May–June 1999 (Table 1) when it was still at southern declinations. The observations of May 24–25, and especially June 4, were inserted in short gaps of the schedule and rely mainly on the absolute pointing of the antenna, which could have been in error by up to $10''$. Therefore the H_2CO observations, which did not yield a detection, will not be considered as the offset may have been as large as the half power beam width of the telescope (Table 2). In fact the SEST $3 - \sigma$ upper limit is less than 25% of the detection of the same line at IRAM for each of the 3 days, and H_2CO was also detected at CSO during May 24–25. The June 4.0 observation of $\text{HCN}(1-0)$ is too noisy to yield a significant result and is ignored because we have better IRAM data from the same day.

The JCMT observations of comet Lee began on May 19 and were spread over four sessions. We also made an unsuccessful attempt to observe it in late October 1999, under poor weather conditions. Pre-perihelion observations were obtained during early evening hours or in the afternoon (June 6–9) when atmospheric instability and primary dish distortion have affected the calibration, by broadening the beam and decreasing its efficiency as well as increasing the pointing uncertainty. The loss in efficiency was determined by regular observations of the same lines in the calibration source IRC+10216 (or OMC-1 for methanol lines) and a correction (+10% to +40%) was applied to the integrated line intensities. A mis-alignment problem of the 230 GHz (A3) receiver in early October resulted in a systematic 25% loss in efficiency, that was precisely measured on Mars and in other line calibration sources. After these corrections, the overall calibration uncertainty of all JCMT observation is estimated to be less than 10%.

CSO observations were limited to early evenings in late May and June, plus three nights in September, after perihelion on July 16. Although the June observations were made under relatively good weather conditions, the comet was very low (elevation of 23° to 15° , and even 7° on the 28th) and the beam efficiency, which is poorly known at such low elevations, may have been significantly overestimated. The other observations (May and September) should have a reliable calibration. Observations at IRAM were undertaken at the same time as some observations on Mauna Kea (June 4–7, in parallel with JCMT, and September 7–10, in parallel with CSO).

Observations at SEST were done in beam-switching mode, with a symmetric throw of $12'$, using two heterodyne receivers simultaneously at 3 mm and 1.3 mm (e.g. to observe HCN(1–0) and CO(2–1)) or 3 mm and 2 mm (HCN(1–0) and CH₃OH at 145 GHz). Either the 210–280 GHz or the 280–370 GHz facility receiver was used at CSO, in beam-switching mode, with a $2'$ throw; the 492 GHz receiver was used to search for the HDO $1_{01} - 0_{00}$ line on May 27, UT. IRAM observations were also conducted in beam-switching mode with the simultaneous use of 3 (at 3 mm, 2 mm and 1.3 mm) or 4 (2 at 3 mm and 2 at 1.3 mm) receivers. Except for some observations of CH₃OH lines at 242 and 338 GHz, most JCMT observations were conducted in frequency switching mode. We either used the A3 heterodyne receiver (220–275 GHz) or the B3 receiver (320–375 GHz, equipped with 2 mixers looking at different polarizations), according to their availability. The total frequency throw used was most of the time close to 16.2 MHz, and switching was done every 30 s in “slow” frequency switching mode or every 2 s in “fast” frequency switching mode with the A3 receiver only. Baseline quality was relatively good in both cases, the main problem being the avoidance of O₃, CO, or HCN atmospheric lines.

The list of observations is given in Table 1 and the frequencies of all the observed lines are given in Table 2, together with the beam sizes of the telescopes with which they were observed. Line intensities are given in the main beam temperature scale, using the beam efficiencies given in Table 3. An extensive atlas of the spectra of HCN, CS, H₂CO, CH₃OH is shown in Figs 1–2, and the single detections of CO and HNC are in Figs 3–4.

Comet C/1999 H1 (Lee) was observed at Nançay with the same technique previously used for other comets (Colom et al. 1999, Gérard 1990, Bockelée-Morvan et al. 1990), but the daily tracking time around transit was reduced to 40 min due to current work on the upgrade of the telescope. The comet was observed (and detected) daily from May 8 to June 20, but observations during July 1 – Aug. 15 did not yield a detection (Table 7), due, in particular, to unfavorable molecular excitation conditions. Sample spectra are given in Fig. 5.

2.1. Ephemerides

The latest available orbital elements, either from the Jet Propulsion Laboratory (JPL/SSD ephemerides, Chamberlin et al.), or the MPCs issued by the Central Bureau of Astronomical Telegrams (Minor Planet Circulars) were used for the observations. Accurate tracking of the comet requires continuous updates of its position, based either on ephemerides computed in real time at IRAM, or interpolated from user-supplied ephemerides. This was not possible with the new version of the telescope control system at CSO in September, and the telescope had to be aimed at a new position every scan, which resulted in a drift of the comet through the beam by $8\text{--}10''$ for each 2.6 to 3.5 min single integration. Ephemeris errors have been computed from the comparison to the orbit based on more recent elements (JPL-DE406 solutions 32 and 37 from January 2000). These errors are given in Table 4, together with the total offset used for the computation of production rates. Systematic pointing errors, if any, are included, and an estimate of the rms pointing error (on the order of 1 to $3''$) was added quadratically to the systematic (pointing + ephemeris) offset.

3. Data Analysis

A wealth of information can be retrieved from the analysis of the observed molecular lines. The relative intensities of the different lines from the same species can be used to derive information on the gas temperature. The shape of the lines reflects the outgassing pattern, and their widths are used to measure the gas expansion velocity. Then we use an excitation and radiative transfer model, as described in Biver et al. (1999b), to derive production rates (Q) from the line integrated intensities. The excitation model of the rotational levels takes into account collisions with water molecules at the local kinetic temperature (T), collisions with electrons (Biver et al. 1999b), and radiative pumping through vibrational or electronic bands. The collision cross-sections (σ_c) are poorly known (in the range $1 - 5 \times 10^{-14}$ cm²) and assumed values are those given in Biver et al. (1999b) with more details on the excitation models in the references therein. Molecular parameters for HDO are those given in Bockelée-Morvan et al. (1998), including a collision cross section $\sigma_c = 5 \times 10^{-14}$ cm². The local density of the water molecules is computed with a Haser model, taking the water production rate $Q_{\text{H}_2\text{O}} \sim 1.1 \times Q_{\text{OH}}$ from Table 7 or $\sim 900 \times Q_{\text{HCN}}$ when no $Q_{\text{H}_2\text{O}}$ or Q_{OH} are available. The electron density is scaled according to the water outgassing rate.

The density of the molecules in the atmosphere of the comet versus distance to the nucleus is described by the Haser model ($n(r) = \frac{Q}{4\pi v_{\text{exp}} r^2} \exp(\frac{-r\beta}{v_{\text{exp}}})$), assuming steady-state radial outflow at the measured expansion velocity (v_{exp}) and a photodissociation rate given by $\beta = \beta_0 r_h^{-2}$. The photodissociation rates β_0 at 1 AU are the same as in Biver et al. (1999b) ($\beta_{0\text{CO}} = 0.065$, $\beta_{0\text{CS}} = 1.0$, $\beta_{0\text{CH}_3\text{OH}} = 1.3$, $\beta_{0\text{H}_2\text{CO}} = 20$ and $\beta_{0\text{H}_2\text{S}} = 25$ in units of 10^{-5} s⁻¹), except for HCN (and for HNC, assumed to be the same), which is more sensitive to solar activity (Bockelée-Morvan & Crovisier 1985), and which was estimated to be around $\beta_{0\text{HCN}} = 2.0 \times 10^{-5}$ s⁻¹ at the time of these observations. For HDO, we assumed a photodissociation rate $\beta_{0\text{HDO}} = 1.3 \times 10^{-5}$ s⁻¹ (Crovisier 1994).

In the case of HNC, the spectroscopic parameters are poorly known due to the instability of the molecule in the laboratory. Here we simply assume that HNC behaves similarly to HCN, with the same photodissociation rate, a dipole moment of 3.05 debyes and infrared pumping through the ν_1 vibrational band ($\nu = 3652$ cm⁻¹, Einstein coefficient $A_1 = 177$ s⁻¹, implying a total excitation rate at 1 AU from the Sun $g_1 = 6.5 \times 10^{-4}$ s⁻¹) and the ν_2 band ($\nu = 464$ cm⁻¹, $A_2 = 3.2$ s⁻¹, $g_2 = 3.7 \times 10^{-4}$ s⁻¹) (Nezu et al. 1998).

The radiative transfer is solved numerically, assuming that the local width of the lines is due to thermal broadening at the kinetic temperature T of the gas. This temperature is assumed to be constant throughout the coma. The observed intensity is thus the result of the convolution of the antenna beam pattern with the density profile and rotational population. Radiative decay and pumping by solar radiation dominate in the outer coma and, unless the collision rate is very high, the observed distribution of the line intensities of a given species can significantly differ from the distribution expected from thermal equilibrium at T .

3.1. Expansion velocity

The gas expansion velocity has been estimated from the half-width at half-maximum intensity ($HWHM$) of the line profiles (plotted in Fig. 6). This half-width has been measured on the blueshifted side of the lines, which corresponds to molecules expanding roughly sunward (the phase angle remained between 19° and 57° throughout the observing period). The observed line profiles present little spectral asymmetry, which justifies the use of an isotropic model in the computation of production rates. Indeed, the largest (negative) significant velocity offsets observed, although indicative of more outgassing towards the Sun, are -0.12 ± 0.02 km s⁻¹ (HCN(3-2), June 4–10), -0.14 ± 0.04 km s⁻¹ (HCN(4-3), Aug. 22–23) and -0.23 ± 0.03 km s⁻¹ (CH₃OH lines at 304 and 307 GHz on Sep. 11). This latter value is not so confident due to some uncertainty on the frequency scale.

A power law fit yields $HWHM = 0.861 \pm 0.019 r_h^{-0.40 \pm 0.09} \text{ km s}^{-1}$, for HCN, CH₃OH and H₂CO lines. Separate fits to pre- and post-perihelion data do not show very significant differences. Modeling of the line shapes shows that thermal broadening accounts for at most 10% of the line width, as was previously suggested by Hu, Larson & Hsieh (1991). Accordingly, we will use an expansion velocity law of $v_{\text{exp}} = 0.8 r_h^{-0.4} \text{ km s}^{-1}$, very similar to that measured in other comets of similar activity (e.g. Hyakutake, Biver et al. 1999b).

3.2. Temperature of the coma and collision rates

The simultaneous observation of several transitions of a given molecular species enables the measurement of a rotational temperature, as explained in Bockelée-Morvan et al. (1994b) in the case of methanol. This species has been observed through several transitions in the same receiver band, which minimizes the effect of calibration uncertainties on the line intensity ratios (Fig. 2). Table 5 gives the rotational temperatures measured from 3 to 8 methanol lines observed simultaneously at 145, 242, 338, and 157 GHz, and from the $2_1A^- - 2_0A^+$ and $4_1A^- - 4_0A^+$ lines observed at CSO in the lower (304.2 GHz) and upper (307.2 GHz) sidebands of the 345 GHz receiver, respectively. Rotational temperatures from quasi-simultaneous observations of different HCN lines were also derived (Table 5), but these measurements are more sensitive to differences in calibration, pointing, beam sizes (Table 2, avoided in the case of the $J(3-2)$ line at CSO and $J(1-0)$ line at IRAM on September 10) and time variability.

The local rotational temperature describing the relative population of a series of rotational energy levels of a given species in the coma of the comet evolves from the kinetic temperature close to the nucleus in the collision-dominated region to some line-dependent “fluorescence temperature” in the outer, radiation-dominated coma. For both CH₃OH and HCN, in the present case, this radiative equilibrium leads to very low rotational temperatures (10 to 15 K), except for the 157 GHz and 304/307 GHz methanol lines. These latter cases are transitions from energy levels that maintain the same population ratios far from the collision region (like the 165 GHz CH₃OH lines in Bockelée-Morvan et al. (1994b)). Thus, the rotational temperature based on these two bands is close to the kinetic temperature of the inner coma and does not depend much on the collision rate.

The CH₃OH bands at 145, 242 and 338 GHz, on the other hand, as well as the HCN lines, provide rotational temperatures that depend mostly on the collision rate (which determines the fraction of molecules in the beam thermalized at the relatively high kinetic temperature) and very little on the kinetic temperature. This is illustrated in Table 5, which gives measured rotational temperatures and the values predicted from three different models with different collision regimes:

- including collisions with electrons ($x_{ne} = 1.0$, multiplying factor of the electron density applied to the default model (Biver et al. 1999b));
- identical, but with electron density divided by 2 ($x_{ne} = 0.5$);
- neglecting collisions with electrons ($x_{ne} = 0.0$).

To model the electron density and temperature radial distribution, we used the *in situ* constraints obtained on comet 1P/Halley (see e.g. Flammar 1991, Cravens 1991 and Xie & Mumma 1992) and scaled it to the water production rate of comet Lee. In summary, in the inner coma, inside the contact surface ($R_{\text{CS}} = 900\text{--}3\,000 \text{ km}$ for $Q_{\text{H}_2\text{O}} = 3\text{--}15 \times 10^{28} \text{ molecules s}^{-1}$), the electron density decreases as $Q_{\text{H}_2\text{O}}^{1/2}/r$, where r is the cometocentric distance, and the electrons are thermalized to the gas temperature ($T_e = T$). Then, the electron temperature rises to about 10 000 K at $r = 2 R_{\text{CS}}$, while the electron density also sharply increases, mostly because of the decrease of the recombination rate with ions: this results in a “pile-up” region (Eberhardt & Krankowsky 1995). Further away, beyond $r = R_{\text{rec}}$ ($R_{\text{rec}} = 3\,500\text{--}7\,700 \text{ km}$ for the same range of gas production rates), the hot electrons density follows

a free outflow law $\propto Q_{\text{H}_2\text{O}}/r^2$. The electron density is further parameterized by a multiplying factor x_{ne} , which allows us to investigate higher or lower electron densities with respect to the default model $x_{ne} = 1$ fitting the Halley data.

We use the same total cross sections for collisions with neutrals as the ones given in Biver et al. (1999b), although their values are poorly known. The molecule–electron collisional cross sections are computed for each transition with the formula of Itikawa (1972), which uses the Born approximation. They significantly depend on the electron temperature, but inside the contact surface ($T = T_e$), they are about two orders of magnitude larger than the assumed neutral–neutral collision cross-sections. Farther from the nucleus, where $T_e \approx 10\,000$ K, the neutral–electron cross section are decreased by more than one order of magnitude but the electron collisional rates are still one order of magnitude larger than the neutral collision rates, mainly because of the large speed of the electrons. Hence, when collisions with electrons are included, this latter process dominates the collisions with neutrals, and the uncertainties on the neutral–neutral cross sections are no longer a concern.

As shown in Table 5, physically acceptable electron densities ($x_{ne} = 1.0$) lead to a relatively good agreement between modeled and observed rotational temperatures. Similar values for the rotational temperature can only be reached when assuming much larger neutral–neutral total cross section. The September observations (Table 5) can be fitted with neutral collisions alone ($x_{ne} = 0$) with total cross sections $\sigma_{\text{HCN}} = 1.5 \times 10^{-12}$ cm² and $\sigma_{\text{CH}_3\text{OH}} = 1.0 \times 10^{-12}$ cm². These are one to two orders of magnitude larger than generally accepted (Biver et al. 1999b, Crovisier 1987, Bockelée–Morvan et al. 1994b).

Thanks to observations of several lines of CH₃OH and HCN in comet Lee, we are thus able to constrain nearly independently the collision rates and the temperature of its coma. However, we have only three reliable estimates of the kinetic temperature. Indeed, as explained above, rotational temperatures derived from lines other than the CH₃OH 157 GHz and 304/307 GHz lines are intermediate between the kinetic temperature and cold fluorescence temperature. For further modeling and production rate determinations, assumptions on the heliocentric variation of the kinetic temperature are thus required. As comet Lee displayed a similar outgassing rate as comet Hyakutake in 1996, we have assumed the $r_h^{-1.5}$ variation found to fit the Hyakutake radio data (Biver et al. 1999b) over a range of heliocentric distances similar to that covered by the present comet Lee observations. Fitting to the temperature constraints given in Table 5 (column 7), we find $T = 80\, r_h^{-1.5}$ K pre-perihelion and $T = 50\, r_h^{-1.5}$ K post-perihelion. For simplicity, we have rounded to the nearest 5 K (as given in Table 5) the values used in the computation of the production rates. The lower post-perihelion temperature may not be surprising: this was also observed in the case of comet Hyakutake and might be due to the lower water production rate post-perihelion (see Section 8), which results in a lower photolytic heating of the coma.

Next, it is possible to constrain the collision rate (i.e., x_{ne}), which better fits all observed rotational temperatures (Table 5). In most cases, and for all HCN observations, including some collisions with electrons is required to fit the data. The HCN lines alone would favor the second model $x_{ne} = 0.5$, while the methanol observations require larger collision rates, with $x_{ne} \geq 1.0$. This HCN–CH₃OH discrepancy is not very large and may be related to the poor reliability of the HCN rotational temperatures. Indeed, the best couple of HCN observations, those made on Sept. 10 with similar beam sizes (Table 5), provides better agreement with CH₃OH. We will adopt the default ($x_{ne} = 1$) electron density model. Adopting a slightly different value would result in marginal differences in the derived production rates. The influence of the temperature on the production rates is discussed in § 5.

4. OH observations and production rates

The comet was observed with the Nançay radio telescope almost every day from May 8 to July 9, July 20 to 25 and August 5 to 15. As stated above, comet Lee could not be detected after June 20. This non-detection could be attributed to the combined effects of smaller inversions of the OH maser, larger

geocentric distances, and to smaller post-perihelion activity.

The observations were made using the same instrumentation and protocol as the previous cometary observations at Nançay (Bockelée-Morvan et al. 1990, Bockelée-Morvan et al. 1994a). The reduction and conversion of the observed signals into OH production rates were made using the same model as before, which takes into account the quenching of the cometary OH maser by collisions. Modeling of the quenching has been improved recently on the basis of the observations of comets Hyakutake and Hale-Bopp (Gérard et al. 1998, Colom et al. 1999), but this improvement is of little consequence for the moderately active comet Lee.

The spectra were averaged over periods of 5 days or more to increase the signal-to-noise ratio. The spectra corresponding to detections are shown in Figure 5. The parameters of the averaged spectra and the corresponding production rates are listed in Table 7.

As explained in Bockelée-Morvan et al. (1990), the OH-parent expansion velocity v_{exp} can be retrieved from the OH line shapes. If one fits a trapezium to the line profile, the half width of the trapezium base (listed in Table 7) is the sum of v_{exp} and v_{eject} , the mean ejection velocity of the OH radical following its parent’s photodissociation. Assuming $v_{\text{eject}} = 1.05 \text{ km s}^{-1}$ from models of water photolysis, we can readily estimate v_{exp} . However, the limited signal-to-noise ratio of the OH spectra does not allow us to investigate the variation of v_{exp} as a function of r_h , as was done from the millimeter lines (Fig. 6). From an average of the OH data over the whole period where the 18-cm lines were detected (spanning $r_h = 0.83$ to 1.39 AU), we obtain $\langle v_{\text{exp}} \rangle = 0.95 \pm 0.04 \text{ km s}^{-1}$. This is to be compared with $\langle v_{\text{exp}} \rangle = 0.82 \pm 0.10 \text{ km s}^{-1}$ from a similar average of the millimeter lines. The larger $\langle v_{\text{exp}} \rangle$ from the OH data may be attributed to the larger beam size of the Nançay telescope, compared to the millimeter telescopes. Hydrodynamical models of cometary atmospheres predict that, as a result of photolytic heating, the parent molecules are accelerated as they expand from the nucleus. The assumed H_2O and OH lifetimes at 1 AU are respectively 8.2×10^4 and $1.1 \times 10^5 \text{ s}$ (Crovisier 1989) and the $\text{H}_2\text{O} \rightarrow \text{OH}$ branching ratio is 90%, implying $Q_{\text{H}_2\text{O}} = 1.1 \times Q_{\text{OH}}$.

OH production rates and upper limits are given in Table 7 and plotted in Figure 7, together with a power law fit to the pre-perihelion data. Post-perihelion observations yield only upper limits, which should be used cautiously as the value of the maser inversion is very uncertain: while the model by Schleicher & A’Hearn (1988) yields similar values (within 15%) as Despois et al. (1981) (Table 7) for pre-perihelion observations, for the August observation the difference implies an upper limit 4 times higher when using the inversion from Schleicher & A’Hearn (1988).

5. Production rates

All production rates have been computed according to the models previously described, assuming symmetrical outgassing at all times with a Haser density distribution, and taking into account the pointing offsets given in Table 4. We also assumed a constant radial expansion velocity and temperature throughout the atmosphere of the comet. The complete excitation model, including collisions with electrons, has been used as previously defined. Carbonyl sulphide (CS) and formaldehyde (H_2CO) are assumed to come from a distributed source with a parent equivalent scale-length $L_p = v_{\text{exp}} r_h^2 \tau_{0p}$: for CS, τ_{0p} is taken to 340 s, corresponding to the CS_2 lifetime (Huebner, Keady & Lyon 1992); for H_2CO , τ_{0p} is taken to $\approx 8000 \text{ s}$ ($\approx 1.6 \times \text{H}_2\text{CO}$ lifetime, following Biver et al. 1999b). Production rates and some significant upper limits are given in Table 6.

The uncertainty in the expansion velocity and its influence on production rates is less than 10%, but the kinetic temperature and collision rates are much less constrained and may have larger impacts on the derived production rates. In the following list, we detail the influence of varying the kinetic temperature (by $\approx 30\%$) and the collision rate (taking into account, or not, collisions with electrons).

- CH_3OH : Neglecting collisions with electrons would reduce all productions rates by 12 to 17%,

except those based on the “thermometer” 304/307 and 157 GHz (and 351 GHz – upper limit) lines, for which the effect is exactly opposite. As a result, this would increase the discrepancy in the production rates based on these two kinds of lines by a factor 2 to 4 when nearly contemporaneous observations exist. For most observations, a +30% (respectively –30%) change in T results in a +(10 – 20)% (respectively –(10 – 20)%) change in production rate (12% on average), but the inverse trend is observed for lines connecting high energy levels, namely the 338 GHz lines and the 241 GHz lines on Oct 1.

- CS: The CS(5–4) line is not very sensitive to the excitation conditions since modifying the collision rates or temperature as previously suggested would not change the production rates by more than 10% (5% on average). Post-perihelion data and especially the CS(7–6) observation (about 2.5 times more sensitive) show opposite behavior to the pre-perihelion ones: increase of Q_{CS} when decreasing the temperature or collision rate. It is interesting to note that HST observations on June 7 UT and August 22 UT (Feldman et al. 1999) yielded CS₂ production rates of $\sim 1 \times 10^{26}$ and $\sim 0.6 \times 10^{26}$ molecules s^{–1}, respectively, when using the same CS₂ lifetime that we adopted in analyzing the radio observations. Thus, the HST and radio production rates agree to within 30%.
- H₂CO: Production rates derived from the 5₁₅ – 4₁₄ line and, to a lesser extent, the September upper limit derived from the 3₁₂ – 2₁₁ line, are almost insensitive (by less than 5%) to a 30% change in the model kinetic temperature. Increasing T by 30% would increase the June 4 production rate based on the 3₁₂ – 2₁₁ line by 20% (and vice versa). Removing collisions with electrons would make less consistent the production rates or upper limits based on the 5₁₅ – 4₁₄ and 3₁₂ – 2₁₁ lines: the corresponding $Q_{\text{H}_2\text{CO}}$ are increased and decreased by about 15%, respectively. Another important parameter is the parent scale-length: if we assume instead that H₂CO is a parent molecule coming directly from the nucleus, then the production rates (and abundances) have to be decreased by $\approx 45\%$ (by up to 64% for the September upper limit);
- HCN (and HNC): Between ~ 0.7 and ~ 1.2 AU from the Sun, the $J(3-2)$ line is the best one for production rate determinations as it shows little sensitivity to the excitation parameters such as the temperature and collision rate. Outside this heliocentric range, inferred production rates are very sensitive to the assumed collision rate x_{ne} , especially as we assumed a low $\sigma_c = 10^{-14}$ cm² neutral–neutral collision cross section: neglecting collisions with electrons enhances by a factor of 2 the production rates based on the HCN(4–3) and HCN(3–2) lines, while decreases by a factor of 2 those based on HCN(1–0). When collisions with electrons are not considered, the production rates derived from the (1–0)/(3–2) lines observed on May 25, differ by 10σ , while a 2σ agreement is obtained when considering collisions with electrons. The discrepancy reaches 15σ for the (1–0)/(3–2) couple of lines observed on Sept. 10, in contrast to the perfect agreement obtained when including collisions with electrons. Clearly, collisions with electrons are a determining excitation process for HCN. As regards to the influence of the kinetic temperature, a change by 30% does not influence any HCN production rate determination by much more than 5%.
- CO: We obtained only one tentative detection of CO at radio wavelengths in this comet (Fig. 3). The production rate derived from this $J(3-2)$ line is, fortunately, not very sensitive to the adopted kinetic temperature, and not at all to the collision rate (Biver et al. 1999b): increasing T by 30% would increase the production rate by 8%. The CO(2–1) line intensity is about twice as sensitive to the temperature, but its observations lead to higher upper limits on relative abundances.

In summary, the acceptable uncertainties on the model parameters are not likely to produce changes in the production rates by more than 20%, thanks to the constraints provided by simultaneous observations of several lines of the same species. The evolution of the production rates and upper limits for the eight species (OH, HCN, CH₃OH, H₂CO, CS, CO, HNC and H₂S) versus date and heliocentric distance is shown in Figure 7. Power law fits to some of the data are also drawn in this figure and reported in Table 6.

5.1. Mean abundances

Table 8 gives the average abundances of the various species studied here, relative to HCN (average of pre- and post-perihelion data) and to H₂O. The water outgassing rate has been computed from OH (Table 7). The most consistent abundances were obtained using the fitted production rate, i.e. $Q_{\text{H}_2\text{O}} = 10.0 \times 10^{28} r_h^{-2.3}$ molecules s⁻¹ pre-perihelion. For determining the CO abundance relative to water from the August 24 tentative detection, we assumed $Q_{\text{H}_2\text{O}} = 6.5 \times 10^{28}$ molecules s⁻¹. This value gives HCN and CH₃OH abundances relative to water in August equal to the pre-perihelion values.

Water has been also detected by other means. From HST observations, Feldman et al. (1999) derive $Q_{\text{H}_2\text{O}} \sim 1.5 \times 10^{29}$ molecules s⁻¹ on June 7 UT (the wings of the OH spatial profile give 1.2×10^{29} molecules s⁻¹, while the core gives 1.8×10^{29} molecules s⁻¹), and $Q_{\text{H}_2\text{O}} = 0.7 \times 10^{29}$ molecules s⁻¹ on August 22 UT. From observations of the 1₁₀-1₀₁ line at 557 GHz performed by the SWAS spacecraft, $Q_{\text{H}_2\text{O}}$ has been estimated to 10^{29} molecules s⁻¹ around May 21 (Neufeld et al. 2000). The HST value for August 22 is in agreement with the assumption we made for deriving the CO relative abundance. On the other hand, HST and SWAS H₂O production rate determinations in May-June are about 50% higher than the value derived from Nançay data, using the power law fit (Table 7). Adopting the SWAS or the HST June water production rate would reduce the abundances relative to water given in Table 8 by 33%. On the other hand, infrared observation of the 1₁₁ – 1₁₀ H₂O line of the ν_3 - ν_2 band on Sep. 2–4, post-perihelion (Weaver et al. 1999), yields a rather low production rate of 2×10^{28} molecules s⁻¹. Using this value and the HCN observation of Sept. 7, we derive a HCN/H₂O ratio about 80% higher than that given in Table 6. Nevertheless, the abundances are within the range found in other comets (Bockelée-Morvan 1997), but with definite differences with those found in comets Hyakutake (Biver et al. 1999b) and Hale-Bopp (Biver et al. 1999a, Bockelée-Morvan et al. 2000):

- Comet Lee is rather depleted in CO. The CO/H₂O mixing ratio is $\sim 4\%$, in agreement with infrared data obtained in September (Weaver et al. 1999). CO was also securely confirmed in the infrared when detected on August 20 with the NIRSPEC spectrometer on the Keck telescope by Mumma et al. (1999), yielding a very similar production rate. Its abundance is 5 times less than the values measured in comets Hyakutake and Hale-Bopp near 1 AU from the Sun.
- Comet C/1999 H1 (Lee) belongs to the “methanol rich” comets (Bockelée-Morvan et al. 1995, Mumma et al. 1993), with a methanol abundance of $\approx 4\%$ relative to water, about twice that found in comets Hyakutake and Hale-Bopp. The CH₃OH/HCN ratio is 3–4 times larger.
- Formaldehyde is also relatively abundant in comet Lee, but its average abundance relative to water of 1.3% is within a factor of 2 the values measured in Hyakutake and Hale-Bopp; the H₂CO/CH₃OH ratio is 25% in comet Lee instead of 50% in comets Hyakutake and Hale-Bopp. On the other hand, we observe a net tendency for the H₂CO/H₂O ratio to be lower post-perihelion (0.8% at 1.12 AU; $< 0.3\%$ at 1.3 AU). The CS to HCN abundance ratio (0.8) is similar to that found in other comets. The HNC/HCN ratio, although similar to that measured in comet Hale-Bopp, was unexpected and will be discussed in the next section.

Upper limits obtained on H₂S and OCS abundances are not very significant as they are comparable, or much higher in the case of OCS, to the highest abundances measured in other comets.

6. Detection of HNC and its implications

The HNC(3–2) line at 271981.142 MHz was detected on two consecutive days at JCMT, June 6.1 and 7.1 UT, with a combined signal-to-noise ratio of ~ 8 . The spectrum in Fig. 4 shows the line and its two “ghost” counterparts at ± 17.9 km s⁻¹, after removal, by Gaussian fitting, of the 0.5 K O₃ atmospheric line at 271926.368 MHz. This frequency switched spectrum was mainly contaminated by the shoulder of the O₃ line ghost counterpart appearing at $+7.7$ km s⁻¹ relative to the comet velocity.

For this reason, there may be some uncertainty in the cometary line intensity due to baseline removal, but, since both its “ghost” counterparts are visible in the folded spectra, the detection is secure.

The HNC observations were bracketed with observations of the HCN(3–2) line on June 6.03, 7.00 and 7.16. Frequent calibration checks were made on IRC+10216 in both HNC and HCN J(3–2) lines to reduce the uncertainty in the HNC/HCN ratio. The uncertainty due to calibration and baseline errors is estimated to be below 30%. Using a line area of 517 ± 27 mK km s^{−1} for the June 6+7 HCN(3–2) observations, the HNC/HCN line intensity ratio is $13.9 \pm 1.7\%$. When taking into account slight differences in beam size and spectroscopic parameters (Section 3), this translates into a HNC/HCN production rate ratio of $12 \pm 2\%$, almost independent of the assumed excitation model parameters. The HNC(1–0) line was also searched for at IRAM at the same time, between observations of HCN(1–0), but the derived $3 - \sigma$ upper limit on the HNC/HCN ratio is 17%.

The HNC/HCN ratio observed in comet Lee at 0.99 AU from the Sun is similar to the value of 14% measured in the active comet Hale-Bopp at ~ 1 AU from the Sun (Biver et al. 1999a, Irvine et al. 1999), and also comparable to the value of 6% found in comet Hyakutake at 1.2–1.1 AU (Irvine et al. 1996). Such a high ratio was quite unexpected. Indeed, from the steep heliocentric increase of the HNC/HCN ratio with decreasing r_h observed in comet Hale-Bopp, it has been proposed, on the basis of chemical models, that HNC is a by-product of coma chemistry transforming some HCN into HNC (Rodgers & Charnley 1998, Irvine et al. 1999). These models, which predict increasing HNC/HCN ratios with increasing water production rates, are not able to reproduce the HNC/HCN ratio observed in the moderately active comet Hyakutake, *a fortiori* the high ratio measured in comet Lee. According to Rodgers & Charnley (1998), the relatively high abundance of methanol in comet Lee would further hinder HNC production in this comet. We thus have to consider the hypothesis that HNC is either a photodissociation product, or a parent molecule. In the latter case, HNC could be of interstellar origin, i.e. synthesized in the proto-solar cloud and not altered in the solar nebula before its incorporation in comets. Unfortunately, the single observation of comet Lee cannot rule out any hypothesis: the HNC line shape is very similar to that of HCN, within error bars: it has a similar blueshift (-0.23 ± 0.09 km s^{−1} for HNC(3–2), -0.16 ± 0.04 km s^{−1} for HCN(3–2)) and is only marginally broader.

7. D/H ratio in water

The $3 - \sigma$ upper limit on the intensity of the HDO $1_{01} - 0_{00}$ line at 464.924 GHz obtained on May 27.2 UT translates into $Q_{\text{HDO}} < 5.6 \times 10^{26}$ molecules s^{−1}. The Nançay data yield an OH production rate of $8.5 \pm 1.7 \times 10^{28}$ molecules s^{−1} for May 27.7 UT, corresponding to $Q_{\text{H}_2\text{O}} = 9.4 \times 10^{28}$ molecules s^{−1}, in agreement with the SWAS determination of $Q_{\text{H}_2\text{O}} = 10.0 \times 10^{28}$ molecules s^{−1} a few days earlier (Neufeld et al. 2000). Therefore, the $3 - \sigma$ upper limit obtained on the HDO/H₂O abundance ratio is $0.6 \pm 0.1\%$, i.e. $\text{D/H} < 30 \times 10^{-4}$. This is ten times higher than the D/H values measured in water in comets P/Halley, Hyakutake and Hale-Bopp (Balsiger et al. 1995, Eberhardt et al. 1995, Bockelée-Morvan et al. 1998, Meier et al. 1998), and also significantly higher than the D/H ratio of $4 - 15 \times 10^{-4}$ measured in interstellar ices (Teixera et al. 1999). Therefore, this upper limit does not produce further constraints on the isotopic exchanges which occurred in the solar nebula (Drouart et al. 1999).

8. Discussion

Following the first ever comprehensive monitorings performed on comets Hale-Bopp and Hyakutake at radio wavelengths (Biver et al. 1997, Biver et al. 1999a, Biver et al. 1999b), comet Lee was the next available opportunity to follow cometary activity over more than four months, extending both before and after perihelion. Although comet Lee did not come as close to the Earth and to the Sun as did comet Hyakutake in 1996, a comparison of the two comets is warranted, since they displayed similar activity levels (the water outgassing rate was only 2–3 times lower for comet Lee) and may have a similar

origin (orbital inclination 149° and period of $\approx 81\,000$ years for Lee versus 125° and period of $\approx 32\,000$ years for Hyakutake).

While we did not obtain detailed information on the evolution of the coma temperature, we were able to obtain precise information on the evolution of the expansion velocity of the gas in the atmosphere of the comet over a factor of more than 2 in heliocentric distance. In addition, the geocentric distance did not vary by more than a factor of 2 (0.72 to 1.52 AU), which limits the influence of the field of view selection effect that may have affected observations of comet Hyakutake in 1996. The general slope of v_{exp} versus r_h (-0.41 ± 0.09 , Fig 6) is not as steep as that found for comet Hyakutake pre-perihelion, but is similar to comet Hyakutake’s post-perihelion behavior. A $r_h^{-0.4}$ behavior has also been observed for Hale-Bopp, both pre- and post-perihelion (Biver et al. 1999a). The mean expansion velocity of 0.8 km s^{-1} at 1 AU is about the same as for Hyakutake.

The production rates of OH, HCN and CH_3OH exhibit an evolution following closely the solar illumination factor r_h^{-2} (Table 6 and 7) pre-perihelion. A steeper evolution $\propto r_h^{-3}$ is observed post-perihelion, resulting in production rates lower, by about 30%, than pre-perihelion at similar (1.2–1.3 AU) heliocentric distances: this rapid decrease of activity with time is similar to that observed for comet Hyakutake and may be due to a short-term aging effect. Cometary nuclei with large obliquity experience fast and pronounced seasonal changes around perihelion. Although we do not know anything about comet Lee’s nucleus, we cannot rule out a seasonal effect that would explain an asymmetric activity with respect to perihelion.

9. Summary

Comet C/1999 H1 (Lee) provided us with a new opportunity to follow the behavior of a comet over a wide range of heliocentric distances, complementing other monitorings at radio wavelengths (1P/Halley, Crovisier & Schloerb 1991; C/1995 O1 (Hale-Bopp), Biver et al. 1997, Womack, Festou & Stern 1997, Biver et al. 1999a; C/1996 B2 (Hyakutake), Biver et al. 1999b).

1. The expansion velocity has been measured to increase as $0.8\text{ km s}^{-1} r_h^{-0.4}$ from 1.7 to 0.8 AU.
2. A rapid “canonical” increase of the OH, HCN, CH_3OH production rates $\propto r_h^{-2}$ was observed from 1.4 to 0.8 AU inbound. A faster decrease $\propto r_h^{-3}$ was observed post-perihelion. In other words, a pre- to post-perihelion asymmetry is observed with lower production rates outbound.
3. HNC has been detected for the third time in a comet, with an HNC/HCN ratio of 12%. This unexpectedly high ratio cannot be explained by the coma chemical models developed to interpret the HNC/HCN ratios measured in comet Hale-Bopp. This raises again the question of the origin of HNC in comets.
4. Comet Lee is rather depleted in CO, while it is rather abundant in CH_3OH . The CO/ CH_3OH ratio of ~ 1 in comet Lee magnifies clear differences in molecular abundances with comets Hyakutake and Hale-Bopp, for which this ratio is 14 and 10, respectively, while all these three comets are thought to have a similar origin.
5. On the other hand, the large abundance of H_2CO close to the Sun is a common characteristic of the three comets. Even if we assume that H_2CO is not released by an extended source, its abundance relative to water in comet Lee is only reduced from $\sim 1\%$ to $\sim 0.5\%$. The H_2CO abundance shows significant temporal variability.

These results demonstrate the need for further measurements of the relative abundances of HNC, CO, and CH_3OH in comets to address the question of their origin and evolution.

We are grateful to observers who kindly gave some of their time for this target-of-opportunity observations (L. Dune and D. Clements at JCMT, E. Falgarone at CSO, S. Sheppard) and to the

JCMT, CSO, SEST and IRAM staff who conducted some of them (T. Lowe and K. Pisciotta at JCMT, A. Sievers and D. Teyssier at IRAM, L. Nyman at SEST). This work was partly supported by the Programme national de planétologie of the Institut national des sciences de l'univers (INSU) and the Centre national de la recherche scientifique (CNRS). The Nançay radio observatory is the Unité scientifique de Nançay of the observatoire de Paris, associated to the CNRS, and also gratefully acknowledges the financial support of the Conseil régional of the Région Centre in France. The James Clerk Maxwell Telescope is operated on behalf of the Particle Physics and Astronomy Research Council of the United Kingdom, the Netherlands Organization for Scientific Research and the National Research Council of Canada. The Caltech Submillimeter Observatory is supported by the National science foundation (NSF) grant AST-9980846. The SEST is operated jointly by the European Southern Observatory and the Swedish National Facility for Radio Astronomy, Onsala Space Observatory at Chalmers University of Technology. IRAM is an international institute cofunded by the CNRS, the MPG (Max Planck Gesellschaft, Germany), and since September 1990 the IGN (Instituto Geografico Nacional, Spain). N. Biver is supported by a fellowship of the James Clerk Maxwell Telescope.

REFERENCES

- Balsiger, H., Altwegg, K., & Geiss, J., 1995, *J. Geophys. Res.*, 100, 5827
- Biver, N., Bockelée–Morvan, D., Colom, P., Crovisier, J., Davies, J.K., Dent, W.R.F., Despois, D., Gérard, E., Lellouch, E., Rauer, H., Moreno, R., & Paubert, G., 1997, *Science*, 275, 1915
- Biver, N., Bockelée–Morvan, D., Colom, P., Crovisier, J., Germain, B., Lellouch, E., Davies, J.K., Dent, W.R.F., Moreno, R., Paubert, G., Wink, J., Despois, D., Lis, D.C., Mehringer, D., Benford, D., Gardner, M., Phillips, T.G., Gunnarsson, M., Rickman, H., Winnberg, A., Bergman, P., Johansson, L.E.B., & Rauer, H., 1999a, *Earth, Moon, and Planets*, 78, 5
- Biver, N., Bockelée–Morvan, D., Crovisier, J., Davies, J.K., Matthews, H.E., Wink, J.E., Rauer, H., Colom, P., Dent, W.R.F., Despois, D., Moreno, R., Paubert, G., Jewitt, D., & Senay, M., 1999b, *AJ*, 118, 1850
- Bockelée–Morvan, D., 1997, in *IAU Symp. 178, Molecules in Astrophysics*, ed. E.F. van Dishoeck (Dordrecht: Kluwer), 219
- Bockelée–Morvan, D., & Crovisier J., 1985, *A&A*, 151, 90
- Bockelée–Morvan, D., Crovisier, J., & Gérard, E., 1990, *A&A*, 238, 382
- Bockelée–Morvan, D., Bourgois, G., Colom, P., Crovisier, J., Gérard, E., & Jorda, L., 1994a, *Planet. Space Sci.*, 42, 193
- Bockelée–Morvan, D., Crovisier, J., Colom, P., & Despois, D., 1994b, *A&A*, 287, 647
- Bockelée–Morvan, D., Brooke, T.Y., & Crovisier, J., 1995, *Icarus*, 116, 18
- Bockelée–Morvan, D., Gautier, D., Lis, D.C., Young, K., Keene, J., Phillips, T., Owen, T., Crovisier, J., Goldsmith, P.F., Bergin, E.A., Despois, D., & Wootten, A., 1998, *Icarus*, 133, 147
- Bockelée–Morvan, D., Lis, D. C., Wink, J. E., Despois, D., Crovisier, J., Bachiller, R., Benford, D. J., Biver, N., Colom, P., Davies, J. K., Gérard, E., Germain, B., Houde, M., Mehringer, D., Moreno, R., Paubert, G., Phillips, T. G., & Rauer, H., 2000, *A&A*, 353, 1101
- Chamberlin, A.B., Yeomans, D.K., Giorgini, J.D., Keesey, M.S., Chodas, P.W., & Bytof, J. (Jet Propulsion Laboratory), JPL's HORIZONS Solar System Data and Ephemerides, <http://ssd.jpl.nasa.gov/horizons.html>

- Colom, P., Gérard, E., Crovisier, J., Bockelée-Morvan, D., Biver, N., & Rauer, H., 1999, *Earth, Moon, and Planets*, 78, 37
- Cravens, T.E., 1991, in *Comets in the Post-Halley Era*, ed. R.L. Newburn Jr, M. Neugebauer, & J. Rahe (Dordrecht: Kluwer), 1211
- Crovisier, J., 1987, *A&AS*, 68, 223
- Crovisier, J., 1989, *A&A*, 213, 459
- Crovisier, J., 1994, *J. Geophys. Res.*, 99-E2, 3777
- Crovisier, J., & Schloerb, F. P., 1991, in *Comets in the Post-Halley Era*, ed. R.L. Newburn Jr, M. Neugebauer, & J. Rahe (Dordrecht: Kluwer), 149
- Despois, D., Gérard, E., Crovisier, J., & Kazes, I., 1981, *A&A*, 99, 320
- Drouart, A., Dubrulle, B., Gautier, D., & Robert, F., 1999, *Icarus*, 140, 129
- Eberhardt, P., & Krankowsky, D., 1995, *A&A*, 295, 795
- Eberhardt, P., Reber, M., Krankowsky, D., & Hodges, R.R., 1995, *A&A*, 302, 301
- Feldman, P.D., Weaver, H.A., A'Hearn, M.F., Festou, M.C., McPhate, J.B., & Tozzi, G.-P., 1999, *BAAS*, 31, 1127
- Flammer, K.R., 1991, in *Comets in the post-Halley Era*, ed. R.L. Newburn Jr, M. Neugebauer, & J. Rahe (Dordrecht: Kluwer), 1125
- Gérard, E., 1990, *A&A*, 230, 489
- Gérard E., Crovisier J., Colom P., Bockelée-Morvan, D., Biver, N., & Rauer, H., 1998, *Planet. Space Sci.*, 46, 569
- Hu, H.-Y., Larson, H.P., & Hsieh, K.C., 1991, *Icarus*, 91, 238
- Huebner, W.F., Keady, J.J., & Lyon, S.P., 1992, *ApJS*, 195, 1
- Irvine, W.M., Bockelée-Morvan, D., Lis, D.C., Matthews, H.E., Biver, N., Crovisier, J., Davies, J.K., Dent, W.R.F., Gautier, D., Godfrey, P.D., Keene, J., Lovell, A.J., Owen, T.C., Phillips, T.G., Rauer, H., Schloerb, P.F., Senay, M., & Young, K., 1996, *Nature*, 383, 418
- Irvine, W.M., Dickens, J.E., Lovell, A.J., Schloerb, F.P., Senay, M., Bergin, E.A., Jewitt, D., & Matthews, H.E., 1999, *Earth, Moon, and Planets*, 78, 29
- Itikawa, Y., 1972, *J. Phys. Soc. Jap.*, 32, 217
- Lee, S., & Garradd, G.J., 1999, *IAU Circ.*7144
- Meier, R., Owen, T.C., Matthews, H.E., Jewitt, D.C., Bockelée-Morvan, D., Biver, N., Crovisier, J., & Gautier, D., 1998, *Science*, 279, 842
- Marsden, B.G., Williams, G.V., & Nakano, S., *Minor Planet Circulars/Minor Planets and Comets, (Central Bureau of Astronomical Telegrams)* <http://cfa-www.harvard.edu/cfa/ps/Ephemerides/Comets/index.html>
- Mumma, M.J., Hoban, S., Reuter, D.C., & DiSanti M., 1993, in *Abstract for IAU Symp. 160, Asteroids, Comets, Meteors 1993*, (Houston: Lunar Planet. Inst.), 227
- Mumma, M.J., Dello Russo, N., DiSanti, M., Gilbert, A.M., Graham, J.R., McLean, I.S., Becklin, E.E., Figer, D.F., Larkin, J.E., Levenson, N.A., Teplitz, H.I., & Wilcox, M.K., 1999, *BAAS*, 31, 3206

- Neufeld, D.A., Stauffer, J.R., Bergin, E.A., Kleiner, S.C., Patten, B.M., Wang, Z., Ashby, M.L.N., Goldsmith, P., Harwit, M., Howe, J., Plume, R., Schieder, R., Snell, R.L., Tolls, V., & Melnick, G.J., 2000, *ApJ*, in press
- Nezu, M., Amano, T., & Kawaguchi, K., 1998, *J. Molec. Spect.*, 192, 41
- Rodgers, S. D., & Charnley, S. B., 1998, *ApJ*, 501, L227
- Schleicher, D.G., & A'Hearn, M.F., 1988, *ApJ*, 331, 1058
- Teixera, T.C., Delvin, J.P., Buch, V., & Emerson, J.P., 1998, *A&A*, 347, L19-L22
- Weaver, H.A., Davies, J.K., Kerr, T., Vacca, W., Biver, N., Bockelée-Morvan, D., Crovisier, J., Brooke, T.Y., Chin, G., & Kim, S.J., 1999, *BAAS*, 31, 1123
- Womack, M., Festou, M.C., & Stern, S.A., 1997, *AJ*, 114, 2789
- Xu, L.-H., & Lovas, F.J., 1997, *J. Phys. Chem. Ref. Data*, 26, 17
- Xie, X., & Mumma, M.J., 1992, *ApJ*, 386, 720

Fig. 1.— HCN lines observed at SEST, JCMT, IRAM and CSO in comet C/1999 H1 (Lee), CS lines observed at IRAM and JCMT (see Fig. 2 for CS(5–4) line in CSO spectra) and formaldehyde lines at CSO, JCMT and IRAM. Telescope, mean observation date and heliocentric distance (r_h in AU) are given for each spectrum. The spectral resolution has been smoothed for some noisy spectra. The intensity scale is main beam brightness temperature, the velocity scale is with respect to the comet rest velocity.

Fig. 2.— Methanol lines observed in comet C/1999 H1 (Lee) at CSO, SEST, IRAM and JCMT. Line identifications are given on the top of each series of spectra. The CS(5–4) is also observed in the upper side band of the two 241 GHz CSO spectra for which we have over-plotted, in dotted line, the low resolution (1 MHz) backend spectra. The JCMT 338 GHz spectra were obtained in two separate 125 GHz subbands plotted here on the same spectrum (the features at 338.450 and 338.595 GHz are band-edge artifacts). Telescope, mean observation date and heliocentric distance (r_h in AU) are given for each spectra. The intensity scale is main beam brightness temperature, the x-axis scale is the velocity with respect to the comet rest velocity for the CH₃OH 304 and 307 GHz lines (actually taken from the same spectra but independently plotted here), or the rest frequency in the comet frame for the other spectra.

Fig. 3.— Observation of the CO(3–2) line in comet Lee in August 1999 (average of 3 days) at JCMT. The spectrum has been binned to a resolution of 0.625 MHz or 0.54 km s^{−1}. The negative feature at $\sim +16$ km s^{−1} is a ghost of the narrow, not removed, CO atmospheric line. Scales are as in Fig.1.

Fig. 4.— HNC(3–2) detection in comet C/1999 H1 (Lee) at JCMT on June 6.1+7.1, 1999 (heavy line) with HCN(3–2) line observed the same days (light dashed line). Vertical scale in main beam brightness temperature is the same for both lines, as well as the horizontal scale which is with respect to the comet rest velocity. Actual (smoothed) resolutions are 0.172 (HNC) and 0.352 km s^{−1} (HCN). Note the “ghost” negative lines of half the total intensity for both HNC (at ± 17.9 km s^{−1}) and HCN (at ± 18.3 km s^{−1}), resulting from the folding of frequency-switched spectra. Ozone (for HNC) and HCN atmospheric main and ghost lines have been removed from the spectra by Gaussian fitting.

Fig. 5.— Sample of OH spectra of comet C/1999 H1 (Lee) obtained with the Nançay radio telescope in May and June 1999: average of both polarizations, 1667 and 1665 MHz lines, scaled to the 1667 MHz one assuming the LTE ratio of 9/5. The lines are in emission as the maser inversion was positive at the time of the observations. The intensity scale is in jansky per beam, the velocity scale is with respect to the comet rest velocity.

Fig. 6.— Evolution of half width at half maximum ($HWHM$) of the molecular lines in comet C/1999 H1 (Lee) as a function of heliocentric distance. Pre-perihelion and post-perihelion data are combined.

Fig. 7.— Evolution of molecular production rates of comet C/1999 H1 (Lee) as a function of heliocentric distance. Left: pre-perihelion data, right: post-perihelion data. The dates corresponding to each step of 0.1 AU are also given on the top scale. Inverted triangles also gives $3 - \sigma$ upper limits, respectively from top to bottom, for OH (3 dates), CO (3), CH₃OH (1), H₂S (1), H₂CO (1) and HNC (1). Power law fits from Table 7 are drawn for OH, HCN and CH₃OH.

Table 1: Log of the observations and line intensities

UT date [mm/dd.dd-dd.dd]	$\langle r_h \rangle$ [AU]	$\langle \Delta \rangle$ [AU]	Integration time [min] ^c	Species	Transition	$\int T_b dv^a$ [K km s ⁻¹]	Resolution [kHz]	Telescope ^b
May 1999:								
05/04.81-06.10	1.437	0.720	428	HCN	1-0	0.045 ± 0.006	80	SEST
05/04.81-05.12	1.444	0.720	188	CO	2-1	< 0.024	80	SEST
05/05.84-06.10	1.429	0.720	240	CH ₃ OH	3 ₀ -2 ₀ <i>E</i>	0.049 ± 0.004	80	SEST
				CH ₃ OH	3 ₋₁ -2 ₋₁ <i>E</i>	0.058 ± 0.005	"	"
				CH ₃ OH	3 ₀ -2 ₀ <i>A</i> ⁺	0.101 ± 0.005	"	"
05/19.24-19.28	1.237	0.839	35	HCN	3-2	0.500 ± 0.079	94	JCMT
05/20.22-20.34	1.222	0.874	121	CH ₃ OH	5 ₀ -4 ₀ <i>E</i>	0.086 ± 0.023	188	JCMT
				CH ₃ OH	5 ₋₁ -4 ₋₁ <i>E</i>	0.100 ± 0.025	"	"
				CH ₃ OH	5 ₀ -4 ₀ <i>A</i> ⁺	0.123 ± 0.028	"	"
				CH ₃ OH	5 ₃ -4 ₃ <i>A</i> ^{±d}	0.057 ± 0.024	"	"
				CH ₃ OH	5 ₁ -4 ₁ <i>E</i>	0.078 ± 0.026	"	"
				CH ₃ OH	5 ₂ -4 ₂ <i>E</i> ^d	0.160 ± 0.028	"	"
05/21.23-21.27	1.209	0.873	37	CH ₃ OH	2 ₁ <i>A</i> ⁻ -2 ₀ <i>A</i> ⁺	0.246 ± 0.037	100	CSO
				CH ₃ OH	4 ₁ <i>A</i> ⁻ -4 ₀ <i>A</i> ⁺	0.451 ± 0.036	"	"
05/22.22-23.28	1.188	0.898	80	CS	5-4	0.098 ± 0.022	100	CSO
				CH ₃ OH	5 ₀ -4 ₀ <i>E</i>	0.062 ± 0.022	1000	"
				CH ₃ OH	5 ₋₁ -4 ₋₁ <i>E</i>	0.120 ± 0.023	100	CSO
				CH ₃ OH	5 ₀ -4 ₀ <i>A</i> ⁺	0.135 ± 0.023	100	"
				CH ₃ OH	5 ₃ -4 ₃ <i>A</i> ^{±d}	0.045 ± 0.026	1000	"
				CH ₃ OH	5 ₁ -4 ₁ <i>E</i>	0.041 ± 0.021	1000	"
				CH ₃ OH	5 ₂ -4 ₂ <i>E</i> ^d	0.060 ± 0.025	1000	"
05/23.98-24.03	1.170	0.921	44	HCN	1-0	0.081 ± 0.018	80	SEST
05/24.21-24.25	1.167	0.925	35	CH ₃ OH	2 ₁ <i>A</i> ⁻ -2 ₀ <i>A</i> ⁺	0.305 ± 0.032	100	CSO
				CH ₃ OH	4 ₁ <i>A</i> ⁻ -4 ₀ <i>A</i> ⁺	0.366 ± 0.034	"	"
05/24.96-25.03	1.157	0.939	56	HCN	1-0	0.060 ± 0.016	80	SEST
05/25.22-26.25	1.146	0.952	70	HCN	4-3	0.560 ± 0.035	100	CSO
				H ₂ CO	5 ₁₅ -4 ₁₄	0.303 ± 0.035	"	"
05/27.23-27.25	1.125	0.979	19	HDO	1 ₀₁ -0 ₀₀	< 0.336	100	CSO
June 1999:								
06/03.83-04.82	1.011	1.147	147	HCN	1-0	0.098 ± 0.010	23,100	IRAM
				H ₂ S	1 ₁₀ -1 ₀₁	< 0.153	23	"
				H ₂ CO	3 ₁₂ -2 ₁₁	0.196 ± 0.019	23	"
06/04.19-04.23	1.015	1.139	38	HCN	3-2	0.510 ± 0.026	94	JCMT
06/05.15-05.19	1.003	1.158	42	CO	2-1	< 0.063	94	JCMT
06/05.60-05.83	0.994	1.170	147	HCN	1-0	0.076 ± 0.007	23,100	IRAM
06/05.60-07.67	0.987	1.185	357	CO	2-1	< 0.040	47,100	IRAM
06/06.03-06.04	0.991	1.176	22	HCN	3-2	0.465 ± 0.040	94	JCMT
06/06.06-07.15	0.983	1.187	194	HNC	3-2	0.072 ± 0.009	94	JCMT
06/06.60-06.83	0.982	1.190	180	HNC	1-0	< 0.015	23	IRAM
06/07.00-07.15	0.978	1.196	37	HCN	3-2	0.580 ± 0.040	94	JCMT
06/07.64-07.83	0.969	1.210	130	HCN	1-0	0.100 ± 0.010	23,100	IRAM
07.68-07.67	0.969	1.210	100	CS	5-4	0.208 ± 0.054	47,100	IRAM
06/08.02-08.15	0.965	1.216	122	CS	5-4	0.107 ± 0.017	94	JCMT
06/09.11-11.28	0.938	1.259	223	CH ₃ OH	5 ₀ -4 ₀ <i>E</i>	0.074 ± 0.019	188	JCMT
				CH ₃ OH	5 ₋₁ -4 ₋₁ <i>E</i>	0.117 ± 0.026	"	"
				CH ₃ OH	5 ₀ -4 ₀ <i>A</i> ⁺	0.092 ± 0.020	"	"
				CH ₃ OH	5 ₃ -4 ₃ <i>A</i> ^{±d}	0.106 ± 0.024	"	"
				CH ₃ OH	5 ₂ -4 ₂ <i>A</i> ⁻	0.078 ± 0.018	"	"
				CH ₃ OH	5 ₃ -4 ₃ <i>E</i>	0.073 ± 0.018	"	"
				CH ₃ OH	5 ₁ -4 ₁ <i>E</i>	0.080 ± 0.019	"	"
				CH ₃ OH	5 ₂ -4 ₂ <i>E</i> ^d	0.172 ± 0.023	"	"
06/09.25-09.28	0.950	1.240	33	HCN	3-2	0.490 ± 0.093	94	JCMT
				HCN ^e	3-2	0.330 ± 0.080	"	"
06/10.25-10.28	0.937	1.260	35	HCN	3-2	0.460 ± 0.070	94	JCMT
06/11.17-11.22	0.926	1.278	43	HCO+	3-2	< 0.15	94	JCMT
				OCS	22-21	< 0.084	"	"
				CH ₃ OH	9 ₀ -8 ₋₁ <i>E</i>	< 0.084	"	"

UT date [mm/dd.dd–dd.dd]	$\langle r_h \rangle$ [AU]	$\langle \Delta \rangle$ [AU]	Integration time [min] ^c	Species	Transition	$\int T_b dv^a$ [K km s ⁻¹]	Resolution [kHz]	Telescope ^b
June 1999:								
06/24.22–27.26	0.778	1.524	100	HCN	3–2	0.310 ± 0.030	100	CSO
06/28.22–28.26	0.755	1.565	43	CH ₃ OH	$2_1A^- - 2_0A^+$	< 0.088	100	CSO
				CH ₃ OH	$4_1A^- - 4_0A^+$	0.107 ± 0.031	“	“
August 1999:								
08/22.64–22.76	1.092	1.329	95	HCN	4–3	0.547 ± 0.044	188	JCMT
08/22.79–22.89	1.093	1.328	90	CS	7–6	0.147 ± 0.033	188	“
				CH ₃ OH	$1_1-0_0A^+$	< 0.097	“	“
08/23.73–23.77	1.106	1.312	30	HCN	4–3	0.603 ± 0.033	188	“
08/22.64–27.84	1.120	1.294	205	CO	3–2	0.036 ± 0.011	188	“
08/24.81–24.84	1.120	1.294	25	H ₂ CO	$5_{15}-4_{14}$	0.183 ± 0.019	188	“
08/25.81–26.92	1.144	1.265	92	CH ₃ OH	$7_{-1}-6_{-1}E$	0.153 ± 0.017	375	“
				CH ₃ OH	$7_0-6_0A^+$	0.182 ± 0.020	“	“
				CH ₃ OH	7_1-6_1E	0.090 ± 0.015	“	“
				CH ₃ OH	$7_2-6_2A^+$	0.068 ± 0.015	“	“
				CH ₃ OH	$7_2-6_2E^d$	0.151 ± 0.019	“	“
September 1999:								
09/06.99–07.35	1.310	1.064	240	HCN	1–0	0.067 ± 0.009	23	IRAM
				CH ₃ OH	$7_0-7_{-1}E$	0.024 ± 0.022	100	“
				CH ₃ OH	$6_0-6_{-1}E$	0.079 ± 0.025	47	“
				CH ₃ OH	$5_0-5_{-1}E$	0.102 ± 0.029	47	“
				CH ₃ OH	$4_0-4_{-1}E$	0.066 ± 0.032	47	“
				CH ₃ OH	$1_0-1_{-1}E$	0.060 ± 0.030	47	“
				CH ₃ OH	$3_0-3_{-1}E$	0.052 ± 0.032	“	“
				CH ₃ OH	$2_0-2_{-1}E$	0.153 ± 0.032	“	“
09/06.99–09.52	1.328	1.043	669	H ₂ CO	$3_{12}-2_{11}$	< 0.045	23	IRAM
09/08.24–08.53	1.328	1.043	190	HCN	1–0	0.062 ± 0.010	23	IRAM
09/08.24–10.50	1.342	1.028	649	CH ₃ OH	3_0-2_0E	0.064 ± 0.006	47	“
				CH ₃ OH	$3_{-1}-2_{-1}E$	0.077 ± 0.006	“	“
				CH ₃ OH	$3_0-2_0A^+$	0.105 ± 0.008	“	“
				CH ₃ OH	$3_2-2_2A^-$	0.022 ± 0.006	“	“
				CH ₃ OH	$3_2-2_2E^d$	0.033 ± 0.006	“	“
				CH ₃ OH	3_1-2_1E	0.026 ± 0.006	“	“
				CH ₃ OH	$3_2-2_2A^+$	0.014 ± 0.006	“	“
				09/09.20–09.52	1.342	1.028	239	HCN
09/10.19–10.50	1.356	1.012	220	HCN	1–0	0.042 ± 0.007	23	“
				CS	5–4	0.097 ± 0.017	23,100	IRAM
09/10.49–10.63	1.359	1.008	115	HCN	3–2	0.162 ± 0.010	100	CSO
09/11.51–11.69	1.374	0.992	164	CH ₃ OH	$2_1A^- - 2_0A^+$	0.234 ± 0.012	100	CSO
				CH ₃ OH	$4_1A^- - 4_0A^+$	0.197 ± 0.010	100	CSO
09/12.52–12.67	1.389	0.977	144	CS	5–4	0.039 ± 0.007	100	CSO
				CH ₃ OH	5_0-4_0E	0.061 ± 0.009	1000	“
				CH ₃ OH	$5_{-1}-4_{-1}E$	0.069 ± 0.006	100	“
				CH ₃ OH	$5_0-4_0A^+$	0.088 ± 0.009	100	“
				CH ₃ OH	5_1-4_1E	0.035 ± 0.010	1000	“
				CH ₃ OH	$5_2-4_2E^d$	0.052 ± 0.012	1000	“
				CH ₃ OH	$5_2-4_2E^d$	0.052 ± 0.012	1000	“
October 1999:								
10/01.31–02.38	1.666	0.830	140	HCN	3–2	0.223 ± 0.012	94	JCMT
10/01.39–02.48	1.667	0.830	170	CH ₃ OH	5_0-4_0E	0.024 ± 0.012	188	“
				CH ₃ OH	$5_{-1}-4_{-1}E$	0.093 ± 0.014	“	“
				CH ₃ OH	$5_0-4_0A^+$	0.107 ± 0.015	“	“
				CH ₃ OH	5_1-4_1E	0.044 ± 0.013	“	“
				CH ₃ OH	$5_2-4_2E^d$	0.074 ± 0.015	“	“
10/24.34–26.28	1.996	1.178	175	HCN	4–3	< 0.049	188	“

^aLine integrated intensity.

^bTelescope used for the observations, CSO-10.4m, or JCMT-15m, or SEST-15m or IRAM-30m antennae.

^cTotal integration time, i.e. ON+OFF in the case of beam-switching.

^dBlended lines (see Table 2).

^eCoarse mapping, average of 7" offsets.

Table 2: Line frequencies and beam sizes

Molecule	Transition	Frequency [MHz]	CSO	Beam sizes SEST or JCMT	IRAM
CO	2-1	230 538.000		21"	10.4"
CO	3-2	345 795.990		13.6"	
HCN	1-0	88 631.847		54"	26.4"
HCN	3-2	265 886.432	27"	18.5"	
HCN	4-3	354 505.472	19.8"	13.2"	
HNC	1-0	90 663.574			25.8"
HNC	3-2	271 981.142		18"	
CS	5-4	244 935.606	28.5"	20"	9.8"
CS	7-6	342 882.995		13.7"	
H ₂ S	1 ₁₀ -1 ₀₁	168 762.762			14.0"
H ₂ CO	3 ₁₂ -2 ₁₁	225 697.775		21.5"	10.6"
H ₂ CO	5 ₁₅ -4 ₁₄	351 768.645	20"	13.4"	
CH ₃ OH	3 ₀ -2 ₀ <i>E</i>	145 093.760		33"	16.2"
CH ₃ OH	3 ₋₁ -2 ₋₁ <i>E</i>	145 097.443		"	"
CH ₃ OH	3 ₀ -2 ₀ <i>A</i> ⁺	145 103.194		"	"
CH ₃ OH	3 ₂ -2 ₂ <i>A</i> ⁻	145 124.334			"
CH ₃ OH	3 ₂ -2 ₂ <i>E</i>	145 126.190 ^a			"
CH ₃ OH	3 ₋₂ -2 ₋₂ <i>E</i>	145 126.392 ^a			"
CH ₃ OH	3 ₁ -2 ₁ <i>E</i>	145 131.873			"
CH ₃ OH	3 ₂ -2 ₂ <i>A</i> ⁺	145 133.418			"
CH ₃ OH	7 ₀ -7 ₋₁ <i>E</i>	156 828.480			15.0"
CH ₃ OH	6 ₀ -6 ₋₁ <i>E</i>	157 048.586			"
CH ₃ OH	5 ₀ -5 ₋₁ <i>E</i>	157 178.962			"
CH ₃ OH	4 ₀ -4 ₋₁ <i>E</i>	157 246.041			"
CH ₃ OH	1 ₀ -1 ₋₁ <i>E</i>	157 270.818			"
CH ₃ OH	3 ₀ -3 ₋₁ <i>E</i>	157 272.320			"
CH ₃ OH	2 ₀ -2 ₋₁ <i>E</i>	157 276.004			"
CH ₃ OH	5 ₀ -4 ₀ <i>E</i>	241 700.168	29"	20"	
CH ₃ OH	5 ₋₁ -4 ₋₁ <i>E</i>	241 767.247	"	"	
CH ₃ OH	5 ₀ -4 ₀ <i>A</i> ⁺	241 791.367	"	"	
CH ₃ OH	5 ₃ -4 ₃ <i>A</i> ⁺	241 832.716 ^a	"	"	
CH ₃ OH	5 ₃ -4 ₃ <i>A</i> ⁻	241 833.104 ^a	"	"	
CH ₃ OH	5 ₁ -4 ₁ <i>E</i>	241 879.038	"	"	
CH ₃ OH	5 ₂ -4 ₂ <i>A</i> ⁺	241 887.678	"	"	
CH ₃ OH	5 ₋₂ -4 ₋₂ <i>E</i>	241 904.158 ^a	"	"	
CH ₃ OH	5 ₂ -4 ₂ <i>E</i>	241 904.643 ^a	"	"	
CH ₃ OH	9 ₀ -8 ₋₁ <i>E</i>	267 403.394		18.4"	
CH ₃ OH	2 ₁ <i>A</i> ⁻ -2 ₀ <i>A</i> ⁺	304 208.324	23.0"		
CH ₃ OH	4 ₁ <i>A</i> ⁻ -4 ₀ <i>A</i> ⁺	307 165.911	22.8"		
CH ₃ OH	7 ₋₁ -6 ₋₁ <i>E</i>	338 344.605		14.0"	
CH ₃ OH	7 ₀ -6 ₀ <i>A</i> ⁺	338 408.718		"	
CH ₃ OH	7 ₁ -6 ₁ <i>E</i>	338 614.953		"	
CH ₃ OH	7 ₂ -6 ₂ <i>A</i> ⁺	338 639.807		"	
CH ₃ OH	7 ₂ -6 ₂ <i>E</i>	338 721.694 ^a		"	
CH ₃ OH	7 ₋₂ -6 ₋₂ <i>E</i>	338 722.914 ^a		"	
CH ₃ OH	1 ₁ -0 ₀ <i>A</i> ⁺	350 950.718		13.4"	
OCS	22-21	267 530.218		18.4"	
HCO ⁺	3-2	267 557.625		18.4"	
HDO	1 ₀₁ -0 ₀₀	464 924.520	15.5"		
Nançay					
OH	F=1-1	1 665.402	3.5' × 19' at Dec. = 0°		
OH	F=2-2	1 667.359	"		

Frequencies are taken from Xu & Lovas (1997) for methanol.

^a indicates blended lines.

Table 3: Telescopes main beam efficiencies

Frequency [GHz]	Telescope beam efficiency			
	CSO	SEST	JCMT	IRAM
89		0.75		0.74
145		0.65		0.54
157				0.51
169				0.49
226		0.50		0.40
230		0.50	0.69	0.39
242	0.65		0.69	
245	0.65		0.69	0.36
266	0.65		0.69	
272			0.69	
305	0.58			
338			0.62	
345			0.62	
351	0.60		0.62	
354	0.60		0.62	
465	0.50			

Table 4: Summary of the observational offsets

UT date [mm/dd.d]	Telescope	Orbital elements used (osculating date)	Pointing offsets in arcsec (O-C) ^a		
			$\Delta(R.A.)$	$\Delta(Dec.)$	total ^b
05/04.9	SEST	JPL-DE406 12	-6.5	+6.1	9.0
05/05.9	"	"	-6.0	+5.5	8.2
05/19.2	JCMT	MPC 34421	-2.5	-5.0	6.3
05/20.2	"	"	-2.6	-5.2	7
05/21.2	CSO	MPC 34421	-2.7	-5.4	6.4
05/22.2	"	"	-2.7	-5.5	6.8
05/23.2	"	"	-2.8	-5.6	6.6
05/24.2	"	"	-2.8	-5.7	6.7
05/25.2	"	"	-2.8	-5.9	7
05/26.2	"	"	-2.8	-6.0	6.9
05/27.2	"	"	-2.8	-6.1	7.0
05/24.0	SEST	MPEC 1999-K10	-1.9	-2.7	4.1
05/25.0	"	"	-1.9	-2.8	4.2
06/04.0	"	"	-1.9	-2.9	4.3
06/04.2	JCMT	JPL-DE406 19 ^c	-2.4	+0.1	2.6
06/05.2	"	"	-2.5	+0.2	3.9
06/06.2	"	"	-2.8	+0.3	3.7
06/07.2	"	"	-3.0	+0.5	3.9
06/08.2	"	"	-3.4	+0.7	4.6
06/09.18	"	"	-3.7	+1.0	4.6
06/09.27	"	"	-3.7	+1.0	4.0
06/10.18	"	"	-4.0	+1.3	4.7
06/10.27	"	"	-4.1	+1.3	4.4
06/11.18	"	"	-4.4	+1.6	7
06/11.25	"	"	-4.4	+1.6	6.1
06/03.8	IRAM	JPL-DE406 17	-2.2	+0.0	2.8
06/04.7	"	"	-2.4	+0.2	3.1
06/05.7	"	"	-2.6	+0.3	3.3
06/06.7	"	"	-2.9	+0.5	3.5
06/07.7	"	"	-3.0	+0.8	3.7
06/24.2	CSO	MPC 34734	+0.8	-2.6	8
06/25.2	"	"	+1.1	-2.6	5.6
06/27.2	"	"	+1.5	-2.8	5.2
06/28.2	"	"	+1.8	-2.9	6.5
08/22.8	JCMT	MPEC 1999-P18	-1.1	+0.2	1.6
08/23.8	"	"	-1.1	+0.2	1.9
08/24.8	"	"	-1.1	+0.3	1.9
08/25.8	"	"	-1.1	+0.4	2.3
08/26.8	"	"	-1.2	+0.4	2.8
08/27.8	"	"	-1.2	+0.4	2.3
09/07.2	IRAM	JPL-DE406 26	-1.2	+1.1	2.6
09/08.4	"	"	-1.2	+1.1	2.6
09/09.4	"	"	-1.2	+1.2	2.6
09/10.3	"	"	-1.2	+1.2	2.7
09/10.5	CSO	JPL-DE406 28 ^c	+1.3	-1.3	4 ^d
09/11.5	"	"	+1.5	-1.5	3.5 ^d
09/12.5	"	"	+1.8	-1.7	3.5 ^d
10/01.4	JCMT	MPC 35814	+0.5	+3.2	4.2
10/02.4	"	"	+0.6	+3.3	4.5
10/24.4	JCMT	MPC 35814	+0.1	+4.8	4.9
10/24.3	"	"	+0.1	+4.8	5.2
10/25.3	"	"	+0.1	+4.8	5.0

^a Observed-Computed position (from JPL-DE406 32 and 37).

^b includes additional pointing errors and rms (1" to 3" typically) of the antenna.

^c Ephemerides for observations were computed from a numerical integration of this orbit.

^d No tracking, comet drifted 8 to 10" across the beam.

Table 5: Temperature measurements

UT Date	r_h (AU)	Molecule	Frequencies (GHz)	Number of lines	Temperatures (K)		Modeled temperatures ^{a,b} (K)			
					Rotational (observed)	Kinetic (constraints)	T	$x_{ne} = 1$ $\Rightarrow T_{rot.}$	$x_{ne} = 0.5$ $\Rightarrow T_{rot.}$	$x_{ne} = 0$ $\Rightarrow T_{rot.}$
May 05.9	1.429	CH ₃ OH	145.1	3	16 ± 2	(14–80)	45	16.1	14.6	12.4
May 20.3	1.222	“	241.8	6	59^{+44}_{-19}	–	60	26.0	23.2	19.9
May 22.8	1.188	“	241.8	6	18^{+6}_{-4}	(14–60)	65	24.5	21.9	19.2
May 22.8	1.188	“	304/307	2	81^{+70}_{-27}	92^{+91}_{-35}	65	59.7	60.3	60.1
Jun.10.2	0.938	“	241.8	8	~ 310	–	90	33.6	30.3	26.4
Aug.25.3	1.143	“	338.6	5	33^{+7}_{-5}	(> 60 ?)	45	24.5	21.5	17.6
Sep.07.2	1.310	“	157.2	7	31^{+8}_{-5}	26^{+9}_{-8}	35	39.4	37.8	36.0
Sep.09.4	1.342	“	145.1	7	20 ± 3	(17–100)	30	21.8	19.4	15.9
Sep.11.6	1.374	“	304/307	2	22 ± 2	23 ± 3	30	32.5	31.8	31.1
Sep.12.6	1.389	“	241.8	5	19 ± 4	(15–100)	30	18.3	16.5	13.9
Oct.01.9	1.667	“	241.8	5	21 ± 4	(> 25)	25	17.3	15.5	12.8
May 25.1	1.15	HCN	88.6/354.5	2	22.3 ± 2.5	–	65	26.7	22.2	14.0
Jun.04.3	1.013	“	88.6/265.9	2	21.3 ± 2.4	–	80	38.3	30.6	15.9
Jun.06.5	0.985	“	88.6/265.9	2	26.6 ± 2.9	–	80	38.8	31.0	16.0
Sep.10.1	1.35	“	88.6/265.9	2	21.4 ± 2.9	–	30	21.3	17.2	9.5

^a x_{ne} : Multiplying factor of the total electron density (1 = default model, 0 = no electrons).

^b $T_{rot.}$: Modeled rotational temperature for assumed x_{ne} and T .

Table 6: Production rates (in units of 10^{26} molecules s^{-1})

UT Date	$\langle r_h \rangle$ (AU)	Q_{HCN}	$Q_{\text{CH}_3\text{OH}}$	$Q_{\text{H}_2\text{CO}}$	Q_{CS}	Others
May 05.5	1.436	0.41 ± 0.06				$Q_{\text{CO}} < 26$
May 05.9	1.429		21.1 ± 1.5			
May 19.3	1.237	0.61 ± 0.10				
May 20.3	1.222		21.6 ± 6.6			
May 22.8	1.188		27.6 ± 3.1		0.64 ± 0.14	
May 24.5	1.163	1.18 ± 0.20				
May 25.7	1.146	0.89 ± 0.06		12.6 ± 1.5		
Jun.04.3	1.013	0.99 ± 0.27				
Jun.04.5	1.010			9.6 ± 0.9		$Q_{\text{H}_2\text{S}} < 9.2$
Jun.05.2	1.003					$Q_{\text{CO}} < 166$
Jun.06.1	0.990					$Q_{\text{CO}} < 56$
Jun.06.6	0.985	1.09 ± 0.19				$Q_{\text{HNC}} = 0.12 \pm 0.02$
Jun.07.7	0.969				0.87 ± 0.22	
Jun.08.1	0.965				0.79 ± 0.13	
Jun.09.3	0.950	0.94 ± 0.14				
Jun.10.3	0.938	1.02 ± 0.15	41.6 ± 24.8			$Q_{\text{OCS}} < 43$
Jun.25.5	0.773	1.77 ± 0.17				
Jun.28.2	0.755		31.8 ± 9.2^a			
Aug.22.8	1.093		< 13		0.69 ± 0.16	
Aug.23.3	1.099	0.71 ± 0.04				
Aug.24.8	1.120			5.6 ± 0.6		$Q_{\text{CO}} = 26 \pm 8$
Aug.25.3	1.143		25.5 ± 4.3			
Sep.07.2	1.310		15.5 ± 7.4			
Sep.08.3	1.327			< 1.1		
Sep.08.8	1.334	0.45 ± 0.05				
Sep.09.4	1.342		14.1 ± 2.7			
Sep.10.2	1.356	0.32 ± 0.01			0.23 ± 0.04	
Sep.11.6	1.374		12.7 ± 2.4			
Sep.12.6	1.389		13.9 ± 0.9		0.30 ± 0.06	
Oct.01.8	1.666	0.22 ± 0.01	8.2 ± 2.3			
Oct.25.3	1.996	< 0.09				
Power law fits:						
Pre-perihelion:		$1.02 \pm 0.09 \times r_h^{-2.0 \pm 0.5}$	$36 \pm 5 \times r_h^{-1.7 \pm 0.6}$		$0.79 \pm 0.06 \times r_h^{-1.2 \pm 0.7}$	
Post-perihelion:		$0.91 \pm 0.22 \times r_h^{-2.8 \pm 0.7}$	$35 \pm 4 \times r_h^{-3.0 \pm 0.3}$		$0.98 \pm 0.62 \times r_h^{-4.1 \pm 2.4}$	

^a Large uncertainty in the beam efficiency (Q probably underestimated).

Table 7: OH observations and production rates

UT Dates [mm/dd.dd–dd.dd]	number of transits	$\langle \Delta \rangle$ (AU)	$\langle r_h \rangle$ (AU)	maser inv. ^a	Line area mJy km s ⁻¹	dV ₀ ^b km s ⁻¹	Q_{OH} 10 ²⁸ s ⁻¹
05/08.76–12.74	5	0.74	1.36	0.34	221 ± 19	2.28 ± 0.25	5.7 ± 0.5
05/13.73–19.71	5	0.82	1.26	0.35	144 ± 13	1.69 ± 0.18	5.8 ± 0.6
05/20.70–24.69	5	0.90	1.19	0.37	133 ± 14	1.97 ± 0.26	4.2 ± 0.5
05/25.68–29.67	5	0.99	1.12	0.40	179 ± 14	2.22 ± 0.22	7.4 ± 0.6
05/30.66–34.65	5	1.09	1.05	0.44	174 ± 16	2.00 ± 0.21	7.1 ± 0.7
06/04.65–08.63	4	1.19	0.98	0.48	204 ± 17	2.46 ± 0.28	8.8 ± 0.7
06/09.63–13.62	5	1.29	0.92	0.50	201 ± 17	2.17 ± 0.22	12.4 ± 1.1
06/14.61–19.60	5	1.40	0.85	0.46	200 ± 15	2.22 ± 0.23	14.4 ± 1.1
06/20.59	1	1.45	0.82	0.39	164 ± 36	1.66 ± 0.52	14.1 ± 3.1
07/01.5–09.5	7	1.64	0.72	-0.27	-20 ± 16	–	< 9.2
07/20.4–25.4	5	1.68	0.75	-0.17	+26 ± 18	–	< 14.8
08/05.3–15.3	9	1.51	0.93	0.13	-18 ± 13	–	< 7.1
Pre-perihelion power law fit:						$9.1 \pm 0.8 \times r_h^{-2.3 \pm 0.6}$	

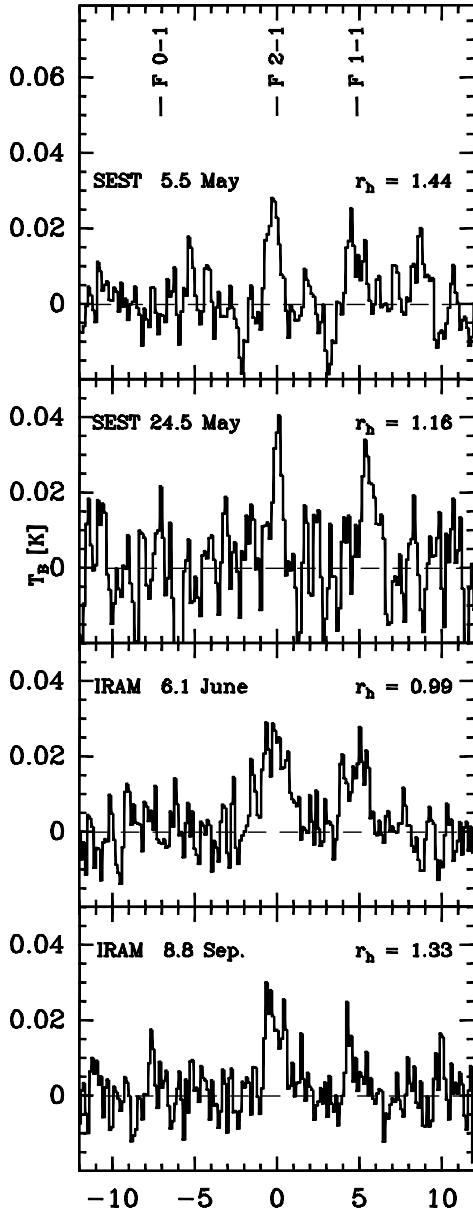
^a A-doublet maser inversion from Despois et al. (1981).

^b Half base of the fitted trapezium (see text).

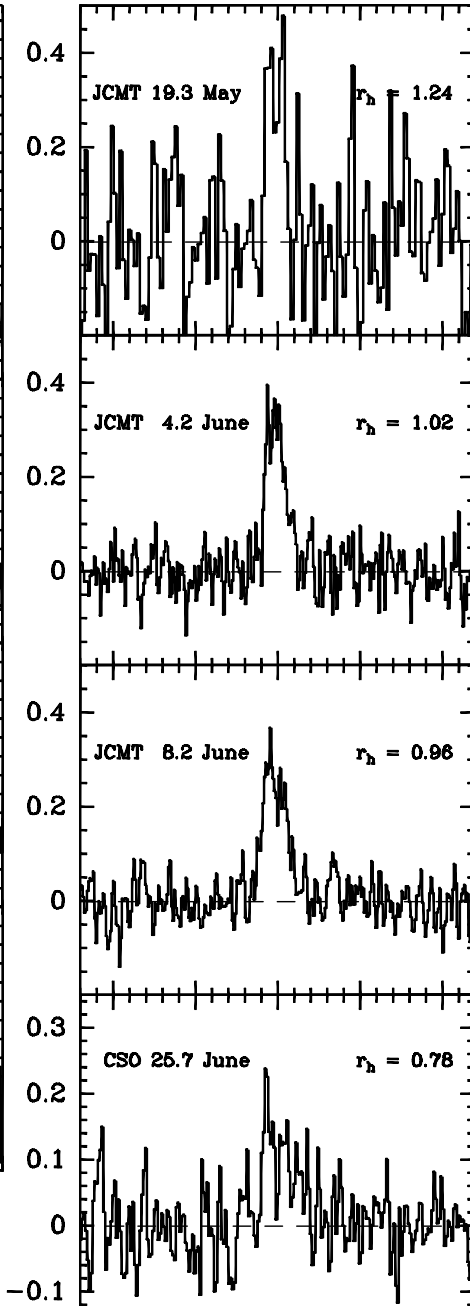
Table 8: Molecular abundances relative to water and HCN

Molecule	$Q_p/Q_{\text{H}_2\text{O}}$	Q_p/Q_{HCN}
HCN	0.11 ± 0.02%	1
CO	4 ± 1 %	37 ± 11
CH ₃ OH	4.0 ± 0.5 %	38 ± 6
CS	0.08 ± 0.01%	0.84 ± 0.09
H ₂ S	< 0.9 %	< 9.3
H ₂ CO	1.3 ± 0.2 %	10 ± 2
HNC	0.012 ± 0.002%	0.13 ± 0.02
HDO	< 0.6 %	< 6
OCS	< 3.6 %	< 42

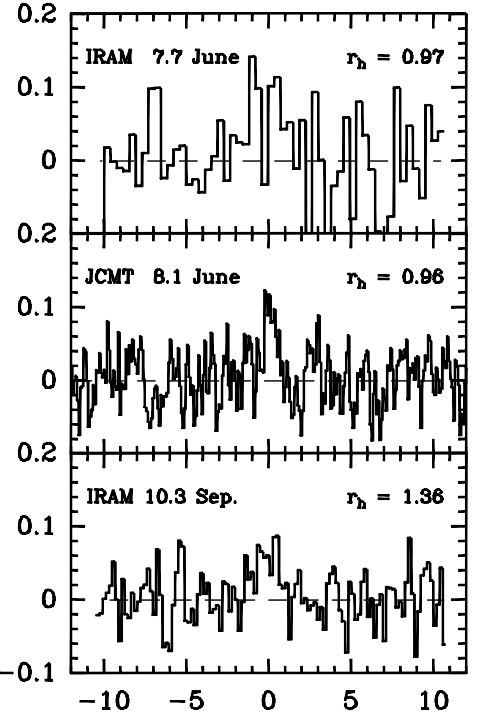
HCN(1-0)



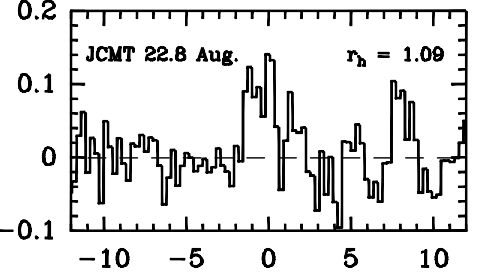
HCN(3-2)



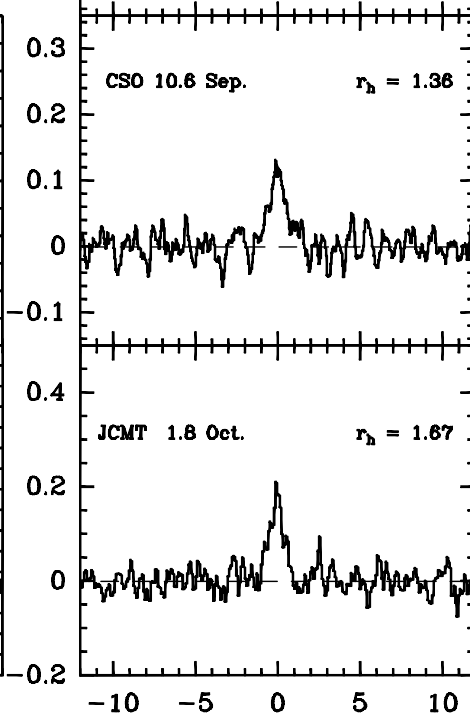
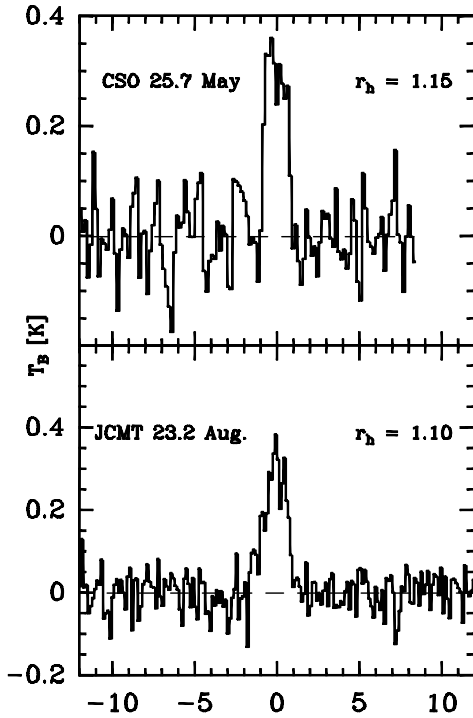
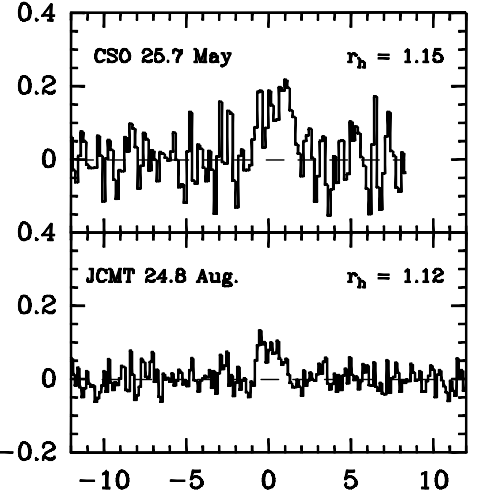
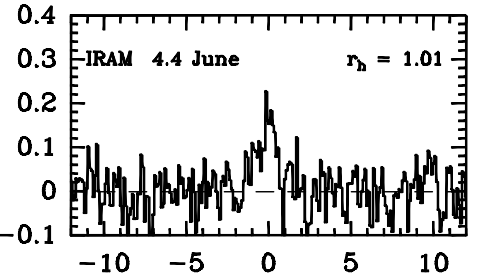
CS(5-4)



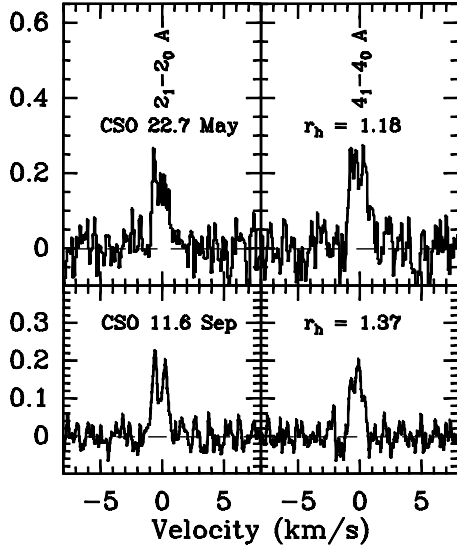
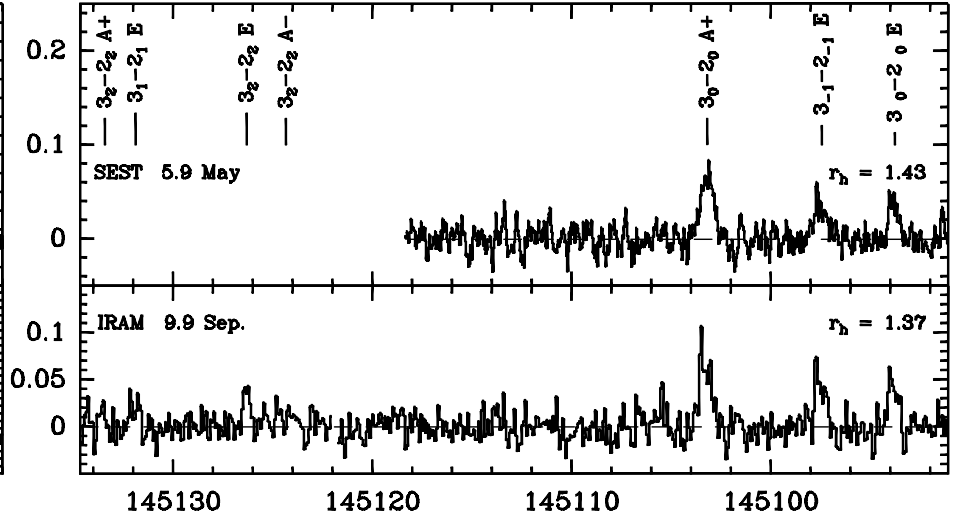
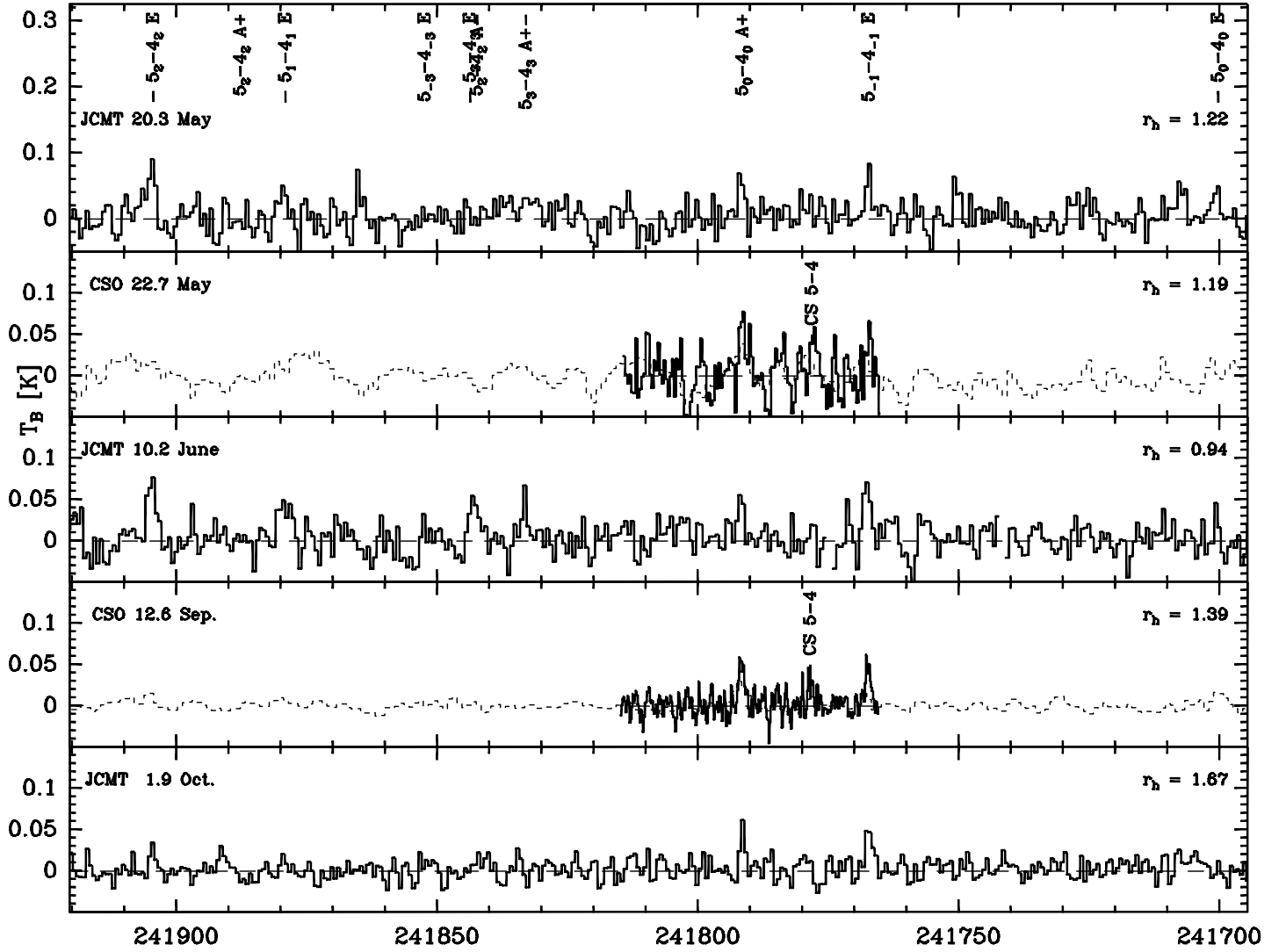
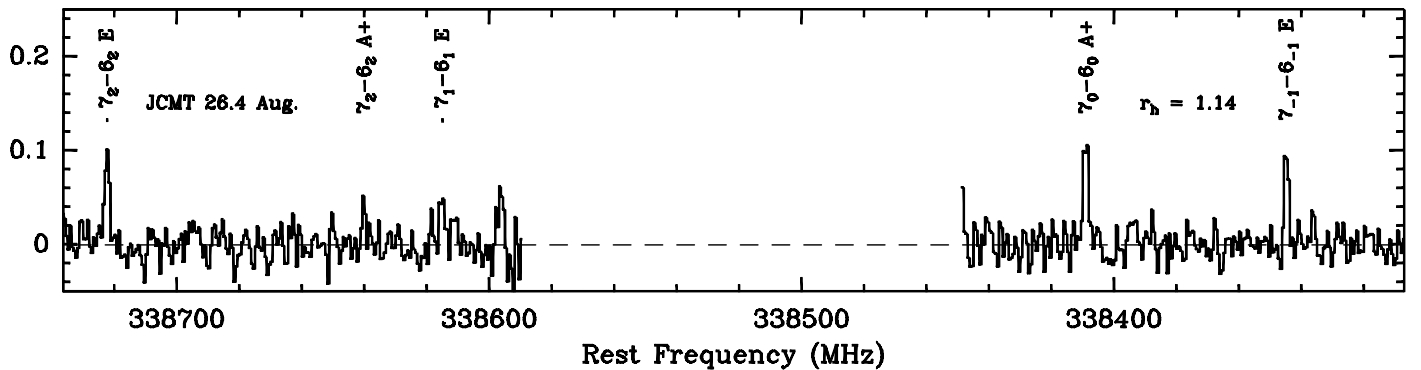
CS(7-6)



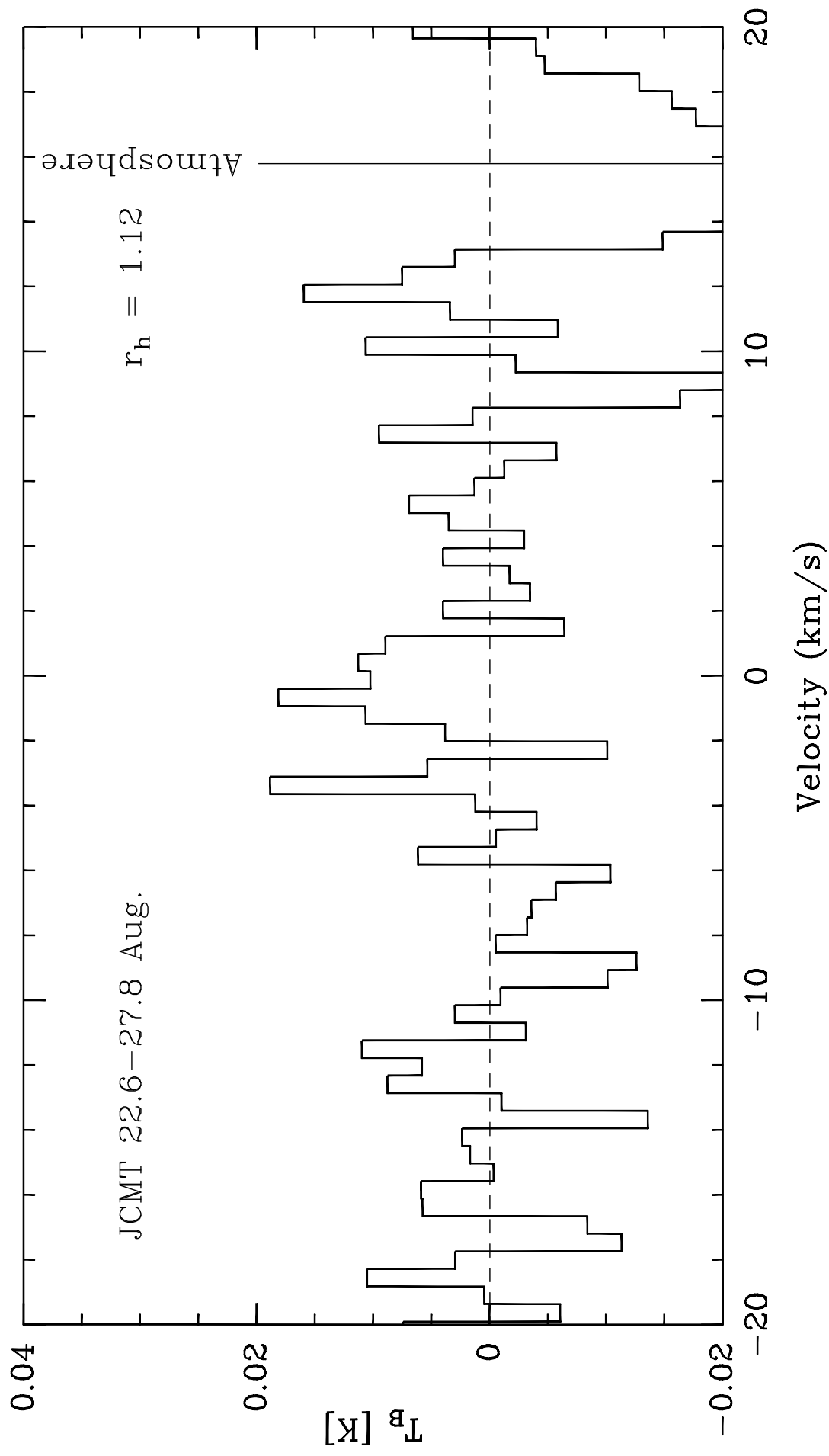
HCN(4-3)

 $H_2CO(5_{15}-4_{14})$  $H_2CO(3_{12}-2_{11})$ 

Velocity (km/s)

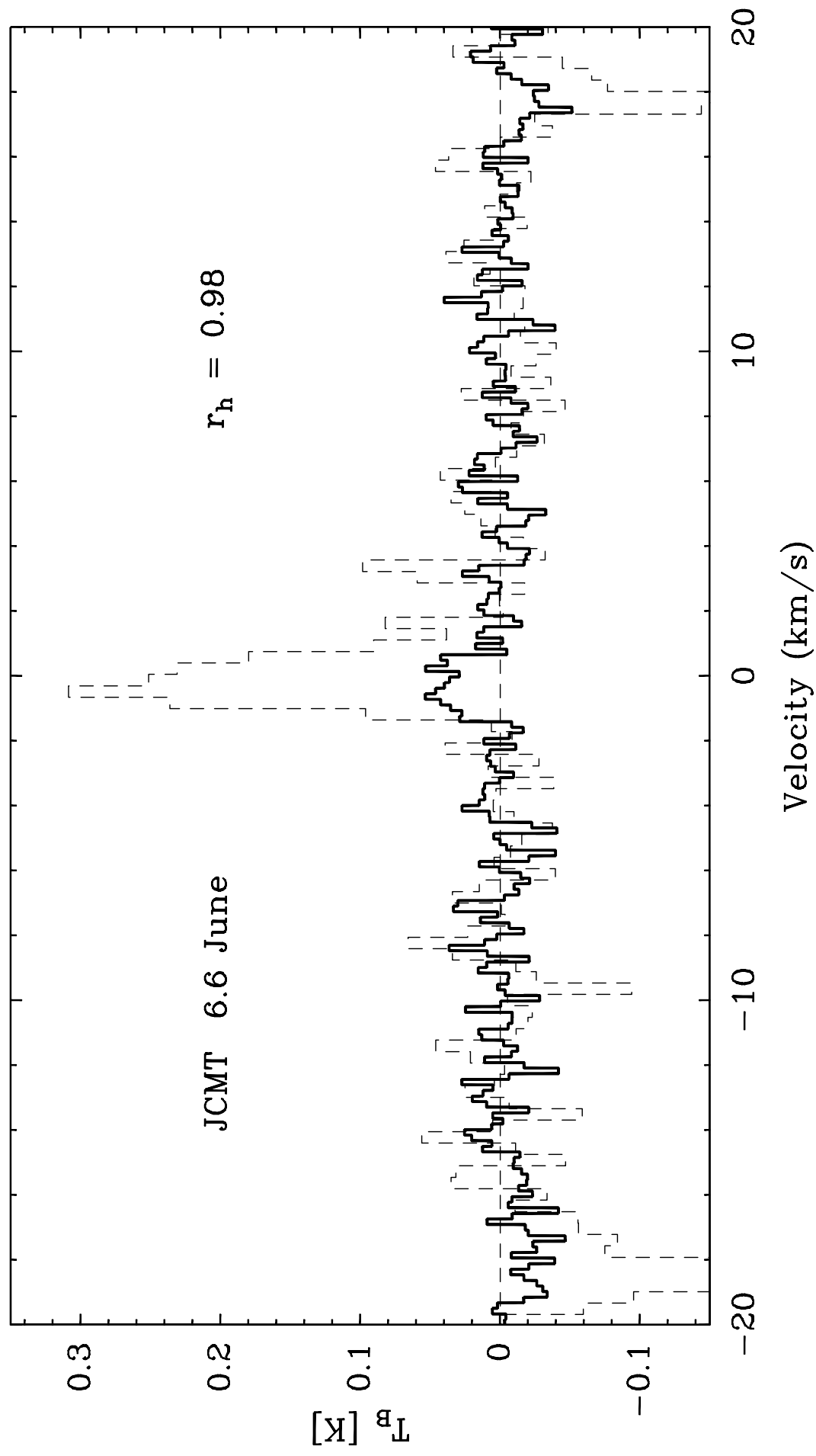
CH₃OH 304/307 GHzCH₃OH 145.103 GHzCH₃OH 241.791 GHzCH₃OH 338.409 GHz

CO(3-2) 345.796 GHz



HNC(3-2) 271.981 GHz

(HNC(3-2) 265.886 GHz)



OH 18 cm

